Significance of stress transfer in time-dependent earthquake probability calculations

Tom Parsons
U.S. Geological Survey, Menlo Park, California, USA

Received 25 May 2004; revised 2 September 2004; accepted 8 September 2004; published 4 March 2005.

[1] A sudden change in stress is seen to modify earthquake rates, but should it also revise earthquake probability? Data used to derive input parameters permit an array of forecasts; so how large a static stress change is required to cause a statistically significant earthquake probability change? To answer that question, effects of parameter and philosophical choices are examined through all phases of sample calculations. Drawing at random from distributions of recurrence-aperiodicity pairs identifies many that recreate long paleoseismic and historic earthquake catalogs. Probability density functions built from the recurrence-aperiodicity pairs give the range of possible earthquake forecasts under a point process renewal model. Consequences of choices made in stress transfer calculations, such as different slip models, fault rake, dip, and friction are tracked. For interactions among large faults, calculated peak stress changes may be localized, with most of the receiving fault area changed less than the mean. Thus, to avoid overstating probability change on segments, stress change values should be drawn from a distribution reflecting the spatial pattern rather than using the segment mean. Disparity resulting from interaction probability methodology is also examined. For a fault with a well-understood earthquake history, a minimum stress change to stressing rate ratio of 10:1 to 20:1 is required to significantly skew probabilities with >80–85% confidence. That ratio must be closer to 50:1 to exceed 90–95% confidence levels. Thus revision to earthquake probability is achievable when a perturbing event is very close to the fault in question or the tectonic stressing rate is low.

Citation: Parsons, T. (2005), Significance of stress transfer in time-dependent earthquake probability calculations, *J. Geophys. Res.*, *110*, B05S02, doi:10.1029/2004JB003190.

1. Introduction

[2] Earthquakes change future seismicity rates in a volume roughly proportional to main shock magnitude. Aftershocks populate parts of the volume, while seismicity might be suppressed in others. Rate changes are temporary; *Omori* [1894] noted that the rate of aftershocks decays with time approximately as t^{-1} following the main shock. Temporary earthquake rate changes can be correlated with static stress changes [e.g., *Harris*, 1998, and references therein]. Most aftershocks are not especially damaging compared to the main shock; however, stress interactions have been correlated with large, damaging earthquakes [e.g., *Kagan*, 1994; *Stein et al.*, 1997; *Parsons*, 2002a]. When empirical observation suggests a major impact on earthquake rates, like the near century long suppression of $M > 6$ earthquakes in northern California following the 1906 earthquake [*Bakun*, 1999; *Harris and Simpson*, 1998], there may be justification for modifying earthquake probability estimates [e.g., *WGCEP*, 2003].

[3] If we want to make a probabilistic earthquake forecast in a region under the influence of past events, then many decisions must be made. We have some observational evidence that stress transfer might hasten or delay another large earthquake. However, time-dependent probability calculations are a means of expressing variability in a poorly understood earthquake renewal process. Often, input parameters are lacking, or must be modeled, and uncertainty mounts. The purpose of this paper is to explore the variability, parameter sensitivity, and limitations of the time-dependent approach and to assess the circumstances under which stress interactions should be added if any.

[4] This effort concentrates solely on the concept of static stress transfer, the theorized lasting change in the stress field resulting from displacements caused by previous fault slip or magmatic intrusions. The significant effects (potentially a minimum 40% of large triggered earthquakes globally [e.g., *Parsons*, 2002a]) from dynamic stress transfer [e.g., *Belardinelli et al.*, 1999; *Kilb et al.*, 2000; *Gomberg et al.*, 2003; *Anderson et al.*, 2003] are not considered here because the physics and timing of dynamic triggering are not well understood.

[5] I draw upon a range of paleoseismic and historic catalogs from the San Andreas fault and Nankai subduction zone to build a thorough picture of the uncertainty and sensitivity of time-dependent probability calculations. From comprehensively studied earthquake ruptures and triggered

This paper is not subject to U.S. copyright.
Published in 2005 by the American Geophysical Union.

events like the 1992 Landers earthquake and the 1999 Izmit-Düzce pair, I assess variability in stress change calculations from source slip models, and receiver fault uncertainties like friction coefficient, dip, and rake. I investigate variability incurred by using different techniques to incorporate stress transfer into probability. Finally, I use simple statistical tools to assess how large a stress change must be (relative to the tectonic stressing rate) to significantly change the distribution of answers from the unperturbed case.

2. Parameter Sensitivity of Time-Dependent Probability Calculations

[6] Time-dependent probability calculations follow the renewal hypothesis of earthquake regeneration such that earthquake likelihood on a fault is lowest just after the last event. As tectonic stress grows, the odds of another earthquake increase. A time-dependent probability calculation sums a probability density function $f(t)$ as

$$P(t \le T \le t + \Delta t) = \int_t^{t+\Delta t} f(t)dt \tag{1}$$

where $f(t)$ can be any distribution, such as lognormal [e.g., *Nishenko and Buland*, 1987], Weibull [*Hagiwara*, 1974], or Brownian passage time [*Kagan and Knopoff*, 1987; *Matthews et al.*, 2002]. These functions distribute around some mean interevent time (μ), and the width of the distributions represents inherent variability (α) on recurrence. For example, a very narrow distribution implies very regular recurrence.

[7] Two commonly applied probability density functions, the lognormal

$$f(t, \mu, \alpha) = \frac{1}{t\alpha\sqrt{2\pi}} \exp\left(\frac{-(\ln t - \mu)^2}{2\alpha^2}\right) \tag{2}$$

and Brownian passage time,

$$f(t, \mu, \alpha) = \sqrt{\frac{\mu}{2\pi\alpha^2 t^3}} \exp\left(-\frac{(t-\mu)^2}{2\mu\alpha^2 t}\right) \tag{3}$$

have characteristics that qualitatively mimic earthquake renewal. The distributions are asymmetric, with less weight at short recurrence time which, when integrated, translates to very low probability early in the earthquake cycle. They are defined by two parameters, mean interevent time, and a coefficient of variation, or aperiodicity that govern their shape. The distributions differ in their asymptotic behavior; integration of the lognormal distribution to very long times asymptotes to zero, whereas the Brownian passage time distribution asymptotes to a fixed value, behavior that *Matthews et al.* [2002] say favors the Brownian distribution for hazard calculations. In this section I explore effects of input parameter variability on time-dependent probability calculation to establish its inherent variation before perturbations from stress transfer are applied.

2.1. Recurrence Interval and Coefficient of Variation

[8] To calculate the time-dependent probability of an earthquake of given magnitude under the renewal model, one must know or estimate its mean interevent time, aperiodicity, and time elapsed since the last earthquake of comparable size. These parameters define the distribution and duration to be integrated, and are most commonly drawn from the historic and paleoseismic record. If an earthquake catalog is lacking, then parameters must be inferred from geologic slip rate and earthquake slip estimates.

2.1.1. Paleoseismic Catalogs

[9] Some of the lengthiest paleoseismic records are found on the San Andreas fault in southern California. At Wrightwood there are 14 events observed [*Fumal et al.*, 2002], and 10 events are noted at nearby Pallet Creek [*Sieh et al.*, 1989]. *Biasi et al.* [2002] calculated an interevent time (μ) of 83 years at Wrightwood with coefficient of variation (α) of 0.70. At Pallet Creek, $\mu = 107$, and $\alpha = 0.76$. Using those parameters, 30-year conditional probability calculated with a lognormal distribution is 40% at Wrightwood, and 30% at Pallet Creek.

[10] Even the longest paleoseismic records are short in the context of building a well-determined distribution. Thus a question emerges. Do the mean recurrence and coefficient of variation from a small sample represent the only distribution that can satisfy the observations? A number of possible approaches can be taken such as Bayesian analysis [e.g., *Ogata*, 1999], data-dependent normalization [*Nishenko and Buland*, 1987], or careful stratigraphic/sedimentological/historical analyses [e.g., *Biasi et al.*, 2002]. The goal here is to find the full array of mean recurrence and coefficient of variation pairs that could satisfy observations, so a forward approach is taken. I constructed Brownian passage time distributions (differences between Brownian and lognormal are explored in a later section) with a range of interevent time and aperiodicity. Events were repeatedly drawn at random from each distribution in an attempt to match the observed event windows (range of possible event times as constrained by radio carbon dating). Distributions that succeeded were tallied (Figure 1). For the Wrightwood and Pallet Creek examples, each distribution was sampled 5 million times, with a number of distributions matching the catalogs at least once (Figures 1 and 2).

[11] Brownian passage time distributions with a range of mean interevent times from 90 to 163 years, and with aperiodicity from 0.4 to 0.9 can match the Wrightwood catalog, and distributions with mean interevent times from 106 to 239 years and aperiodicity from 0.5 to 0.9 can match the sequence at Pallet Creek (Figures 1 and 2). Observed in the paleoseismic [*Sieh et al.*, 1989; *Fumal et al.*, 2002] and historic catalogs, the $M \sim 7$ 1812 and $M \sim 8$ 1857 [*Ellsworth*, 1990] earthquakes attest to significant magnitude variation within the record. This may be part of the reason for the interevent time variability in the catalogs, and for why multiple distributions can fit the observations.

[12] Thirty-year time-dependent probability calculations were made using a Brownian passage time density function from the array of distributions that met observations at Wrightwood and Pallet Creek. Two approaches are possible; one can take the mean of all interevent time distributions that reproduced the catalogs ($\mu = 116$ years, $\alpha = 0.70$ for the Wrightwood case) and calculate one answer (33% in 2004). Alternatively, a histogram of all the probability calculations

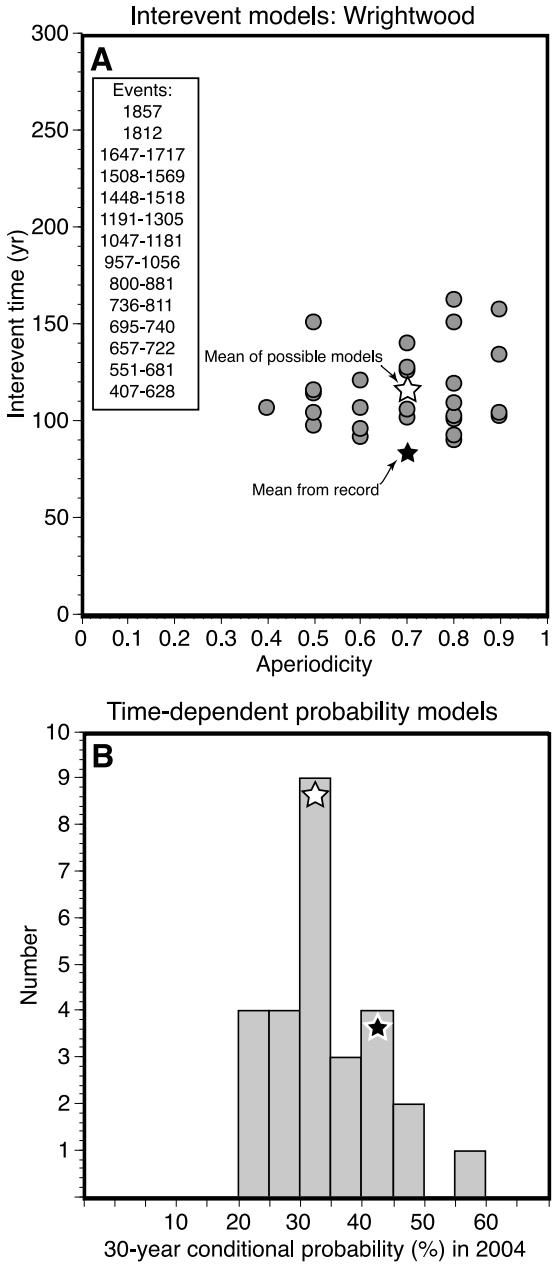

Figure 1. (a) Interevent and aperiodicity combinations that reproduce the earthquake sequence (time ranges shown in inset) on the San Andreas fault at Wrightwood [*Fumal et al.*, 2002] using Brownian passage time distributions. The mean of the combinations is shown as a white star, and the mean taken directly from the data [*Biasi et al.*, 2002] is shown as the black star. (b) Histogram of conditional 30-year earthquake probabilities calculated from the interevent time-aperiodicity pairs using the Brownian model.

can be produced (Figures 1b and 2b). At Wrightwood, a histogram shows that probabilities range from 20% to 60% with a peak between 30 and 35%. That result differs slightly from the probability value (41%) calculated from the $\mu = 83$ and $\alpha = 0.70$ parameters derived from the record by *Biasi et al.* [2002]. Similar results are obtained for the Pallet Creek example; the mean parameters from all the models ($\mu = 162$ $\alpha = 0.72$) lead to a 30-year probability of 24% in 2004, and the histogram plot suggests allowable answers ranging from 15 to 40%

[13] Interpretation of a range or distribution of earthquake probability calculations remains an open issue. Equally viable 30-year probability calculations of 20% and 60% are obtained from a very good paleoseismic catalog at

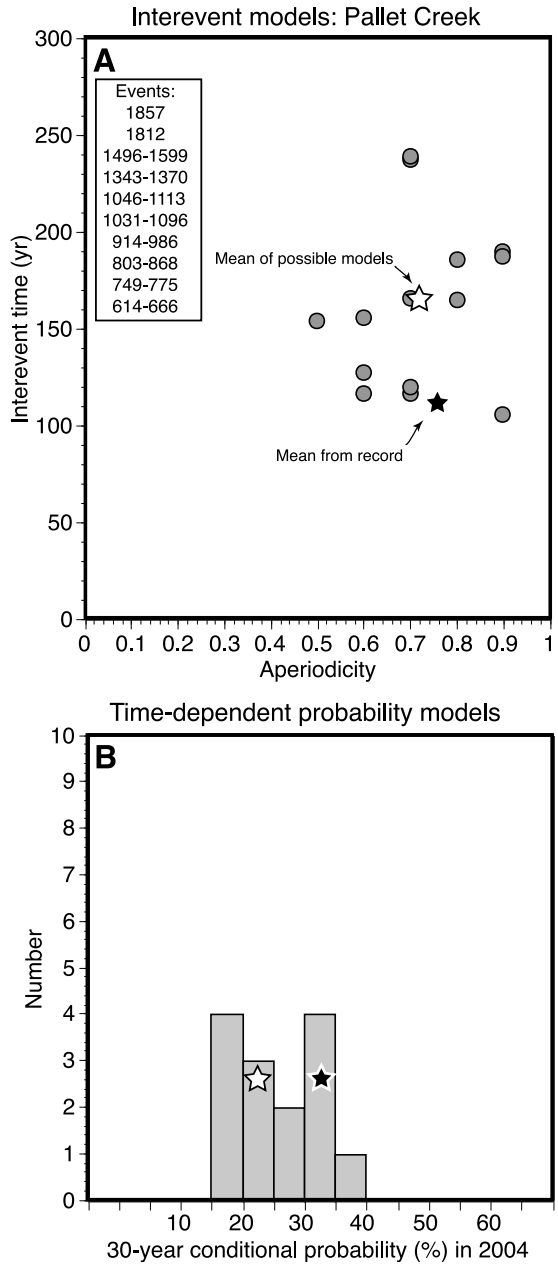

Figure 2. (a) Interevent and aperiodicity combinations that reproduce the earthquake sequence on the San Andreas fault at Pallet Creek [*Sieh et al.*, 1989] using Brownian passage time distributions. The mean of the combinations is shown as a white star, and the mean taken directly from the data [*Biasi et al.*, 2002] is shown as the black star. (b) Histogram of conditional 30-year earthquake probabilities calculated from the interevent time-aperiodicity pairs using the Brownian model.

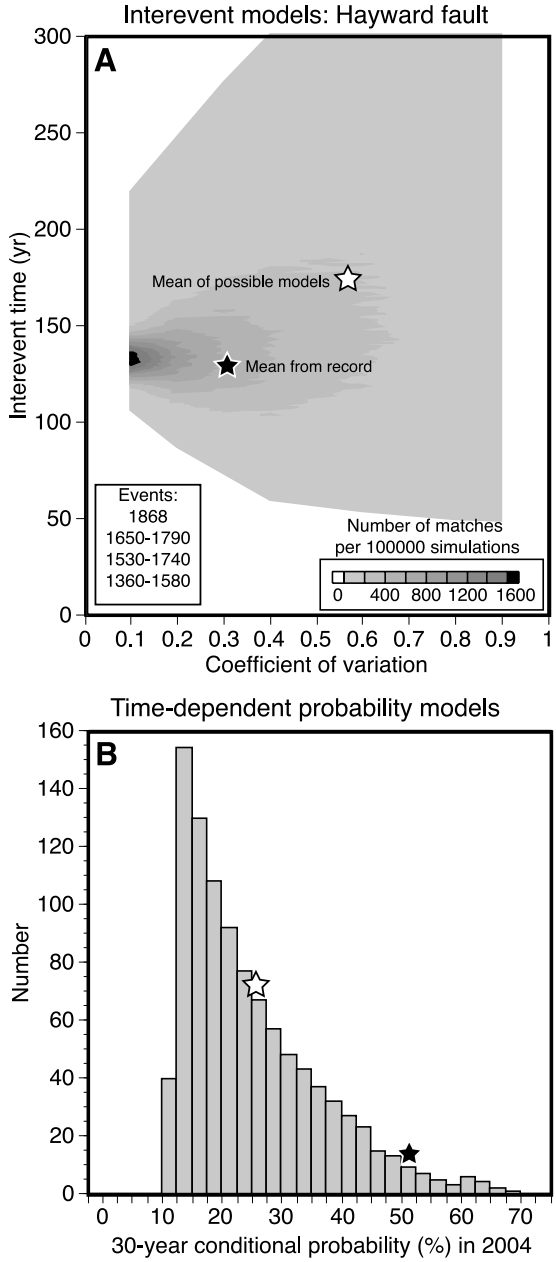

Figure 3. (a) Interevent and aperiodicity combinations that reproduce the earthquake sequence on the southern Hayward fault [*Lienkaemper et al.*, 2002] using Brownian passage time distributions. The shorter sequence can be fit with more models; thus the number of matches is contoured. The mean of the combinations is shown as a white star, and the mean taken directly from the data is shown as the black star. (b) Histogram of conditional 30-year earthquake probabilities calculated from the interevent time-aperiodicity pairs using the Brownian model.

Wrightwood. Most of the results fall between 30 and 35% (Figure 1), which might be a reasonable criterion for selecting a value to report. In this paper I carry all the possible answers forward as a distribution, and test whether stress transfer alters the shape in a significant way.

[14] The examples from Wrightwood and Pallet Creek are relatively long earthquake catalogs (10–14 events). A similar analysis can be carried out for shorter catalogs. For example *Lienkaemper et al.* [2002] report four events over the past ~500 years at Tyson's Lagoon on the south Hayward fault in northern California. A shorter catalog can be more readily fit by an array of interevent time-aperiodicity models. A contour plot is shown in Figure 3a of matches to the record resulting from 100000 draws from Brownian passage time distributions. Distributions with a range of aperiodicity from 0.1 to 0.9 and interevent times from 50 to >300 years can reproduce the catalog. The resulting 30-year probability calculations cover a broad range from 10 to 70% (Figure 3b). These results indicate that the 500-year south Hayward fault catalog is too short to provide parameters for meaningful time-dependent earthquake probability calculations. A 2000-year earthquake catalog from Tyson's Lagoon with 12 events is in development [*Lienkaemper et al.*, 2003] that will substantially improve parameter estimation.

2.1.2. Historical Catalogs

[15] In parts of the world where written records have been kept for a long time relative to large-earthquake interevent times (i.e., Japan, Turkey, Greece), earthquake timing in catalogs can be more tightly constrained, often to the day and hour [e.g., *Usami*, 1988; *Ambraseys*, 2002]. However, historical reporting alone does not often allow for very accurate earthquake locations, which usually must be obtained from isoseismal or other relative intensity methods [e.g., *Bakun and Wentworth*, 1997]. For example, a 2000-year catalog from the Sea of Marmara region of Turkey [*Ambraseys*, 2002], only provides enough intensity detail to locate earthquakes over the past ~500 years [*Parsons*, 2004]. Along the Nankai-Tokai subduction zone in Japan there is a combined paleoseismic and historic earthquake/tsunami record. There, a long and tightly constrained catalog in time and space was developed [*Ishibashi and Satake*, 1998]. The catalog shows considerable complexity with events occurring only at Nankai or Tokai, and others rupturing both zones simultaneously. Attempts to match either the Nankai or Tokai record with multiple interevent models was not possible even with 10 million random draws from each distribution. Thus drawing a mean directly from the data could represent the limited range of possible models. However, significant aperiodicity is expected since there appear to be several instances of coupled earthquakes [e.g., *Lu et al.*, 1999], and interactions between events. A partial analysis of combined Nankai-Tokai ruptures examines four events (Figure 4), but like the short Hayward fault catalog, there is a wide range of possible interevent-aperiodicity pairs that can replicate the catalog, even when the exact rupture date is known.

2.2. Effects of Unknown Elapsed Time Since the Last Event

[16] The earthquake catalogs examined so far have all been associated with at least one historic earthquake. There are important fault zones for which probabilistic analysis is desired, but where there has not been an observed earthquake. For example, the north Hayward and Rodgers Creek faults have not slipped over most of their length since the establishment of Spanish missions in 1776. That date combined with paleoseismology brackets the last large

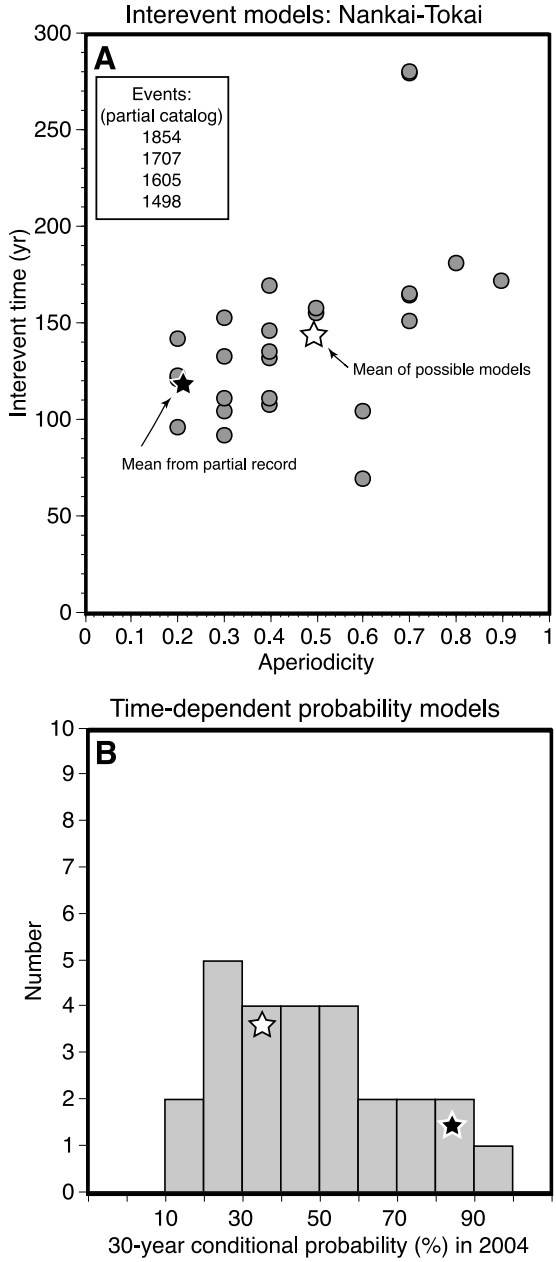

Figure 4. (a) Interevent and aperiodicity combinations that reproduce part of historical earthquake sequence at the Nankai-Tokai trough [*Ishibashi and Satake*, 1998] using Brownian passage time distributions. All events could not be fit with this approach, which signifies a well-constrained catalog. The mean of the combinations is shown as a white star, and the mean taken directly from the data is shown as the black star. (b) Histogram of conditional 30-year earthquake probabilities calculated from the interevent time-aperiodicity pairs using the Brownian model.

earthquake between 1640 and 1776 [*Schwartz et al.*, 2001; *WGCEP*, 2003]. Uncertainty on elapsed time adds to the distribution of calculated earthquake probabilities for a fault segment; drawing at random from dates between 1640 and 1776 for elapsed time on the north Hayward-Rodgers Creek segment while keeping other parameters fixed adds about a 6% range of 30-year probability for the segment (Figure 5). The asymmetry in the distribution of probability in Figure 5 results from integration of the probability density function that returns nearly constant values (30% in this case) for recurrence times greater than the mean.

[17] Another way to examine the effects introduced by elapsed time uncertainty is to use the Wrightwood catalog and pretend that our knowledge of the 1812–1857 events is restricted to their occurrence sometime within the 19th century. By drawing from a range of distributions as before to get all possible interevent time and aperiodicity models, the range of 30-year probability values is broadened to 15–65% (Figure 6). An alternative way to handle uncertain elapsed time is provided by the Brownian passage time model, which can treat the fault state as equal to the Poisson rate with the same interevent time [*Matthews et al.*, 2002]. Also, *Ogata* [1999] developed a weighted average procedure for forecast when the last event time is unknown.

2.3. Probability Distribution Functions

[18] Choice of a probability density function can have a direct influence on the calculated value for a given fault or region. Unfortunately, this decision is somewhat arbitrary because there is little quantitative basis for making it. Differences in the 30-year probability values at any given time are evident between the distributions (Figure 7). At times exceeding one interevent time (μ) disparity among the distributions becomes most important; integration of the Weibull distribution rises monotonically, whereas the lognormal and Brownian distributions rise to a maximum value controlled by the coefficient of variation or aperiodicity. At very long times relative to μ, conditional lognormal probability approaches zero. Under the same conditions the

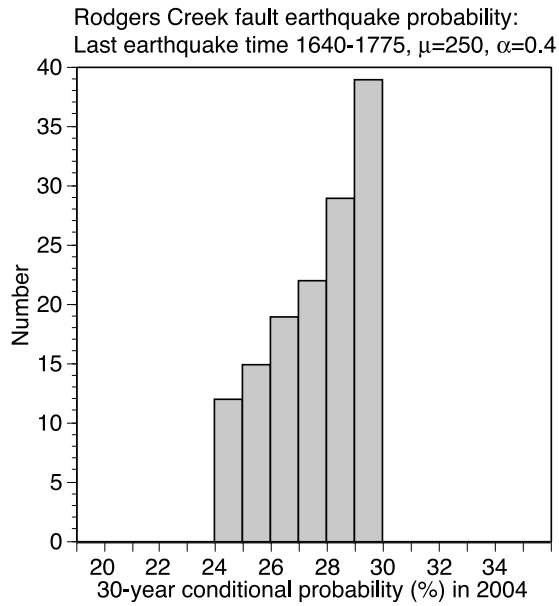

Figure 5. Histogram of probability for fixed interevent time and aperiodicity but variable time elapsed since the last earthquake. This plot indicates about 6% variability introduced by a window of possible last earthquake times between A.D.1640 and 1775.

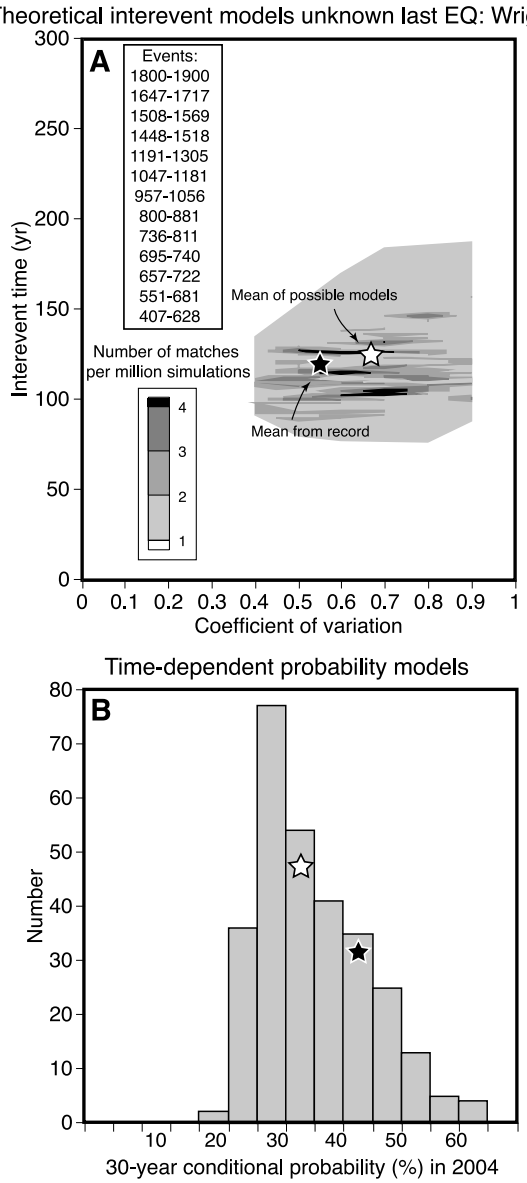

Figure 6. Broadening of possible probabilities for a simulated case at Wrightwood if the last earthquake was not known from historical observation but instead was determined from the paleoseismic catalog alone.

Brownian passage time probability approaches a fixed value; when $\alpha = 1/\sqrt{2}$, the fixed value is the same as the Poisson probability [*Matthews et al.*, 2002]. This behavior is illustrated in Figure 7 where the mean value of $\alpha = 0.7$ from the Wrightwood distributions is used, which is almost equal to $1/\sqrt{2}$.

[19] To investigate the effects of probability density function choice, the same analysis of the earthquake catalog at Wrightwood was conducted except that instead of drawing at random from Brownian distributions, log-normal distributions were used. Somewhat different results were obtained. The mean value of interevent time (μ) from all the distributions was reduced from 116 years to 96 years, and the aperiodicity (α) was reduced from 0.70 to 0.64 (Figure 8a). The histogram of resulting 30-year probabilities has a less peaked shape and smaller range (25–60% compared with 20–60%) (Figure 8b).

2.4. Conclusions Regarding Time-Dependent Probability Parameter Sensitivity

[20] Even long paleoseismic catalogs permit a broad array of equally viable earthquake probability forecasts. In some cases the array appears to have a central peak that might provide some basis for expressing a preferred value [e.g., *Savage*, 1991, 1992], but in others not. Time-dependent probability calculations may not be warranted for paleoseismic catalogs with fewer than ~10 events. Choice of probability density function and knowledge of elapsed time are shown to have potentially broadening effects on the array of probabilities. In the following sections, stress transfer is introduced to the calculations to investigate how large it must be to skew the array of probabilities.

3. Stress Change Calculations

[21] In this section, inherent variability and uncertainty from stress change calculations are explored because their influence on earthquake probability scales with their magnitude. At present, direct measurements of induced stress changes are not made. Instead, slipping (or opening) a dislocation in an elastic half-space simulates the static change in the stress field [e.g., *Okada*, 1992]. Probability changes might also be calculated from stress changes imparted by magmatic intrusions or other forces. Changed stress tensor components are resolved on planes of interest and related to triggering or inhibition of future earthquakes. Usually, the Coulomb stress change is calculated to explain patterns of seismicity change [e.g., *Harris*, 1998, and references therein]. The Coulomb failure criterion ($\Delta\tau$) is defined by

$$\Delta\tau \equiv \left|\Delta\bar{\tau}_f\right| + f_c(\Delta\sigma_n + \Delta p) \tag{4}$$

where $\Delta\bar{\tau}_f$ is the change in shear stress on the receiver fault (set positive in the direction of fault slip), f_c is the coefficient of friction, $\Delta\sigma_n$ is the change in normal stress acting on the receiver fault (set positive for unclamping), and Δp is pore pressure change.

[22] Calculated stress changes depend on parameters that must be estimated, or worse, guessed. Equation (4) above requires an estimate of fault friction, and some concept of pore fluid behavior. There are additional uncertainties involving the earthquake or magmatic source model and its translation to a slipping or opening dislocation. In addition, there are different ways of considering the target faults. One common method is to make calculations on optimally oriented fault planes, which are determined from an input regional stress field and the perturbations caused by the source earthquake. An alternative method is to resolve stresses on known faults, which requires estimates of their strike, dip, and rake. In general probability changes are sought for specific fault segments, thus determining strike, dip, and rake is preferred.

3.1. Slip Model Variation

[23] The source time function of a large earthquake may be determined from geodesy, seismology, or a combination.

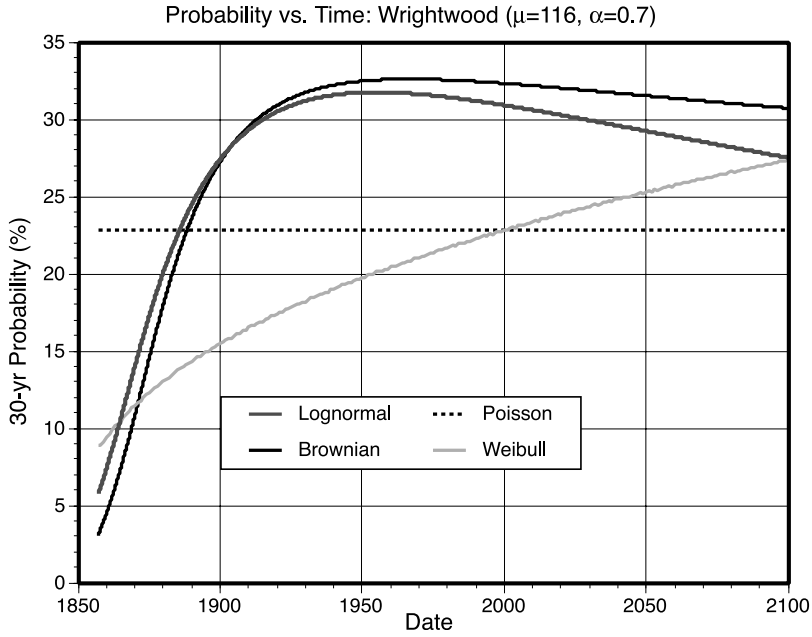

Figure 7. Comparison of 30-year conditional earthquake probability versus time for four density functions using the mean interevent time and aperiodicity values from the Wrightwood catalog.

An estimate of the cumulative slip distribution is needed to make static stress change calculations. Methods are sensitive to different aspects of the earthquake source, and it is not uncommon to have a range of slip estimates resolved on different planes (Figure 9a). Slip model variability was shown to be most important very close to the rupture by *Steacy et al.* [2004]. In this section, a well-studied example, the 17 August 1999 M = 7.4 Izmit, Turkey earthquake is used to investigate variability of stress change calculations because there are multiple slip models, the earthquake apparently triggered the 12 November 1999 M = 7.2 Düzce event, and postseismic strain effects have been studied.

[24] Five estimates of Izmit coseismic slip are considered here [*Reilinger et al.*, 2000; *Wright et al.*, 2001; *Bouchon et al.*, 2002; *Delouis et al.*, 2002; *Li et al.*, 2002], three of which are depicted in Figure 9a. The obvious differences in rupture dimensions and slip distribution cause variation in calculated stress change (Figure 9b), particularly on faults close to the rupture plane (Figure 10). As an example, the Düzce fault was projected from its surface trace on a 60° dip (at a −160° rake) determined from centroid moment tensor solutions of the Düzce earthquake. Stress changes were resolved on the plane using a friction coefficient of 0.2 with five different slip models (Figure 10). Significant variation in the stress change pattern on the Düzce plane is evident, most resulting from slip distribution on the eastern ends of the Izmit source models, and how close slip approaches, or even overlaps the Düzce plane. Effects of source slip model variation coupled with variation in target fault friction, rake, and dip are investigated in section 3.2.

3.2. Friction Coefficient, Rake, and Dip

[25] The 12 November 1999 M = 7.2 Düzce earthquake nucleated at a point calculated to have been stressed by the Izmit event [*Hubert-Ferrari et al.*, 2000; *Parsons et al.*, 2000] and seems a likely example of a large, triggered earthquake. The Düzce hypocenter is thus used here as a test point to investigate stress change calculation variability. Static stress changes were calculated at the hypocenter with varying friction and a range of rakes that encompassed oblique normal to pure strike slip (−140°–180°) with five source models (Figure 11). The effects of frictional variation alone caused 20–50% variation in calculated stress change, depending on the source slip model. Rake variation caused an additional 20% to 80% change in the calculated Coulomb stress at the Düzce hypocenter. Combined variation of friction coefficient and rake caused stress change values to differ between 23% and 127%, depending on slip model (Figure 11). This variation could be reduced with more information about the Düzce fault. For example, if sufficient microseismicity catalogs exist, then it may be possible to correlate stress change calculations with different friction coefficients against seismicity rate changes [e.g., *Reasenberg and Simpson*, 1992; *Parsons et al.*, 1999]. Similarly, if sufficient focal mechanisms can be calculated, then the range of possible rakes might be limited as well.

[26] A span of friction coefficient between 0 and 0.8 is considered here, which is making a common assumption that pore fluid response to static stress change is encompassed within that range. That assumption could well be incorrect [*Beeler et al.*, 2000], since it is not known how fault fluids are distributed, or how they respond to static stress change. Friction coefficient is treated as $f_c' = f_c(1 - B_k)$, where B_k is Skempton's coefficient. Implicit within that assumption is that fault zone porosity is distributed anisotropically, with fluids occupying a shear fabric parallel to slip. In that case, the cracks respond primarily to the stresses acting normal to them [e.g., *Scholz*, 1990] and shear stresses do not contribute to pore pressure

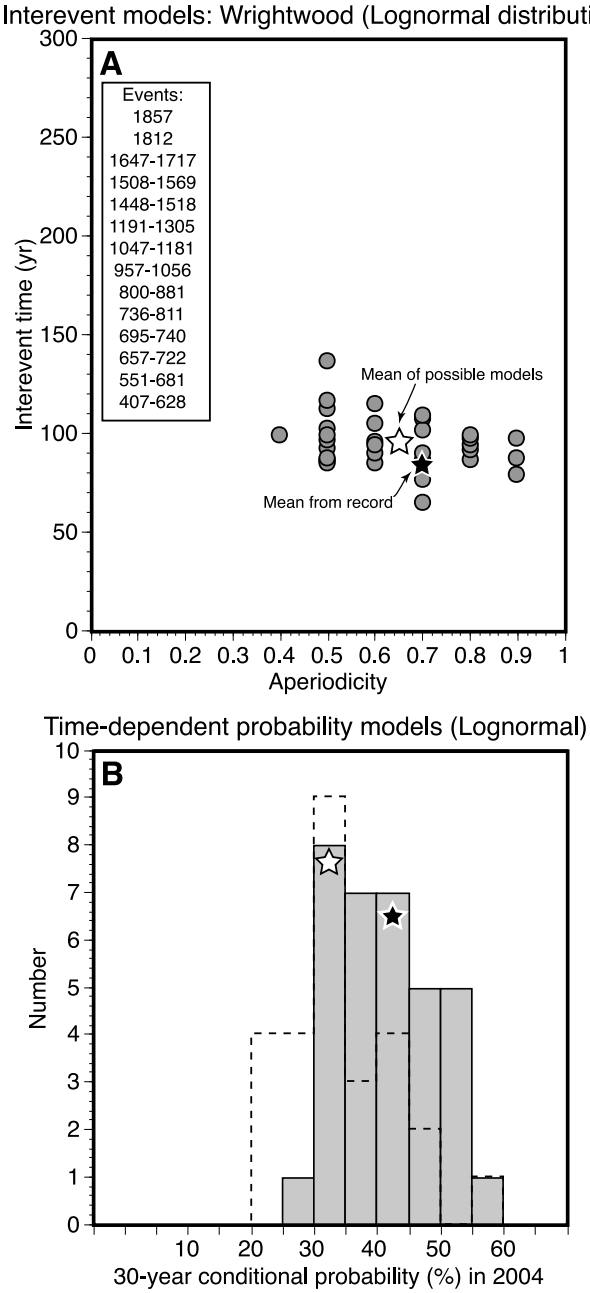

Figure 8. Same approach to finding all possible interevent and aperiodicity combinations that reproduce the Wrightwood earthquake sequence as shown in Figure 1, except that lognormal distributions are used. The dashed black line in Figure 8b shows the Brownian passage time results of Figure 1 for comparison.

changes. Under those conditions the coefficient of friction simplification of pore fluid changes can be used for Coulomb failure.

[27] An additional source of stress change calculation uncertainty is that the dip of a target fault may only be known approximately. Either it is projected from the surface, defined by earthquake hypocenters, identified with seismic reflection profiling or other structural information, or defined by moment tensors or focal mechanisms. In all cases there are uncertainties that lead to variation in stress change calculations. For example, if fault dip at the Düzce hypocenter is allowed to vary from 45° to 90°, then stress change values can vary between 40 and 50%, depending on friction coefficient (Figure 12).

3.3. What Stress Change Value to Use When Forecasting Nucleation at an Unknown Site?

[28] Making stress change calculations for earthquake probability highlights another issue. What value should be used? Should it be the mean stress change, or the peak stress change? In the Düzce hypocenter examples above, the triggered earthquake location was already known. For fault segment earthquake probabilities all that is typically known in advance is that the next earthquake is expected to nucleate somewhere along a lengthy fault plane. We do not know how tectonic stress is distributed, and often have no information about asperities. Inherent uncertainties in calculating either the mean or peak stress are expected. In this section it is shown that for large fault planes, it is common for most of the segment to be stressed by a nearby earthquake at values lower than the mean stress change; if the mean value is used everywhere on the segment, then the probability perturbation would likely be overstated. Thus stress change values for earthquake probability calculations should be pulled from some distribution that reflects calculation uncertainties and the spatial pattern of the stress change.

[29] Returning to the Izmit-Düzce example, we can pretend that the Düzce event has not yet happened and we do not know where or when large earthquake nucleation will occur. Coseismic static stress changes calculated on the Düzce fault are shown in Figure 10; peak stress changes tend to be near the west end of the fault and decline to the east. Since stress on most of the fault is only slightly increased and the areas of peak stress are localized, the vast majority of potential nucleation sites are increased to degrees less than the mean stress increase (Figure 13a). A distribution of all the stress-increased fault patches (2.5 × 0.5 km) is plotted scaled against the mean stress increase. This distribution characterizes the calculated state of post-Izmit stress change encompassing variation from five different Izmit slip models and unknown Düzce fault friction and rake (Figure 13a). Most of the stress increases are normally distributed between ~0 and the mean with a standard deviation between 0.25 and 0.5. The same analysis conducted just for the Düzce hypocenter shows stress changes normally distributed about the mean, with standard deviation between 0.15 and 0.25 (Figure 13b), which gives an impression of just the effects of slip model and target fault uncertainties.

[30] If we assume that nucleation could occur anywhere on the Düzce plane, then we might draw stress change values at random from this distribution to calculate probability change. However, the actual Düzce earthquake nucleated near the peak stress change part of the fault. Thus perhaps drawing from the stress change values above the mean would be a better choice. This issue will be visited in section 5, where statistical significance of probability changes is assessed.

3.4. Postseismic and Viscoelastic Loading

[31] Deep postseismic afterslip and viscoelastic relaxation of the lower crust and upper mantle may redistribute

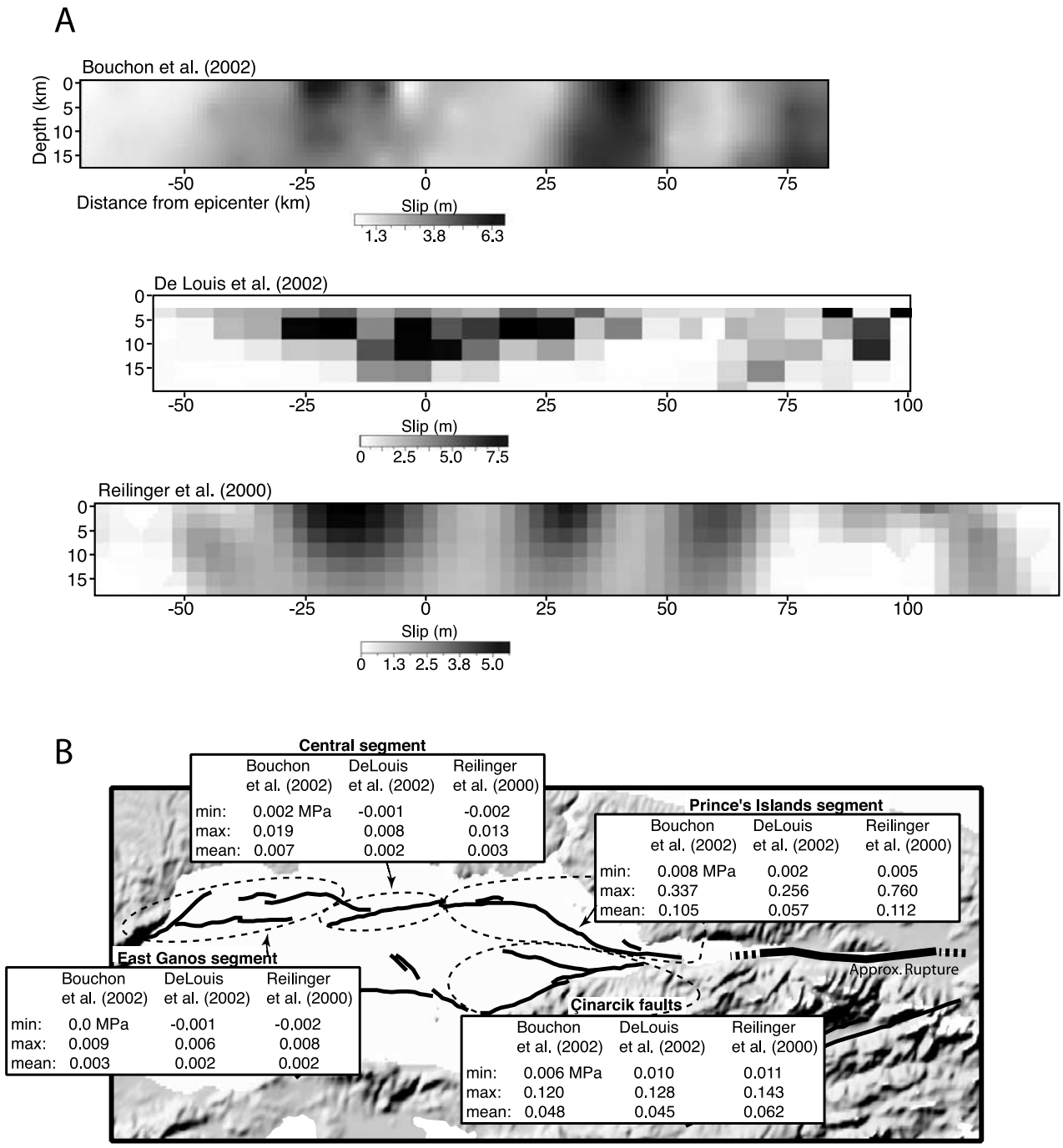

Figure 9. (a) Modeled slip distribution of the 17 August 1999 M = 7.4 Izmit earthquake from three different studies. Coseismic slip in meters is contoured on the fault surfaces. The origin of the models is the Izmit epicenter. (b) Differences in calculated Coulomb stress change for different fault segments adjacent to the Izmit rupture resulting from use of the three slip models shown in Figure 9a.

stress into the seismogenic crust over time [e.g., *Nur and Mavko*, 1974; *Savage and Prescott*, 1978] affecting the likelihood of earthquake nucleation. Surface deformation following the Izmit earthquake was modeled by postseismic afterslip and creep in the lower crust and/or upper mantle [*Bürgmann et al.*, 2002], and calculated to have increased stress at the Düzce hypocenter [*Hearn et al.*, 2002] (Figure 14). A simple way to incorporate afterslip in probability calculations is to combine the coseismic and postseismic slip models [*Parsons*, 2004].

4. Incorporation of Stress Transfer Into Probability Calculations

4.1. Recurrence Interval Change Versus Clock Change

[32] A direct way to incorporate calculated stress changes into earthquake probability calculations is to

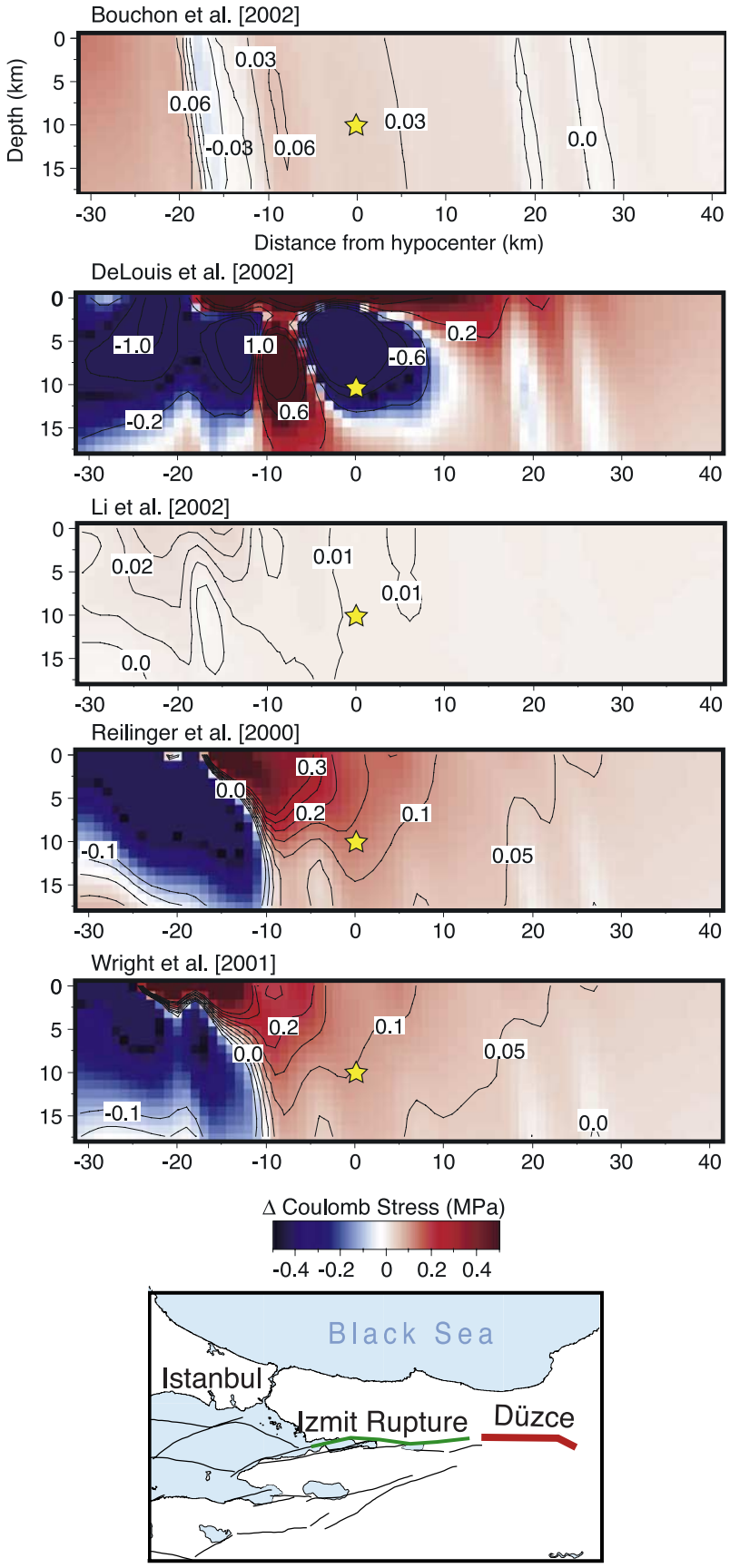

Figure 10. Calculated changes in Coulomb stress from different Izmit slip models projected onto a 60° dipping Düzce fault surface projected from the mapped trace. Friction coefficient $f_c = 0.2$, and a rake of $-160°$ was used for the calculations.

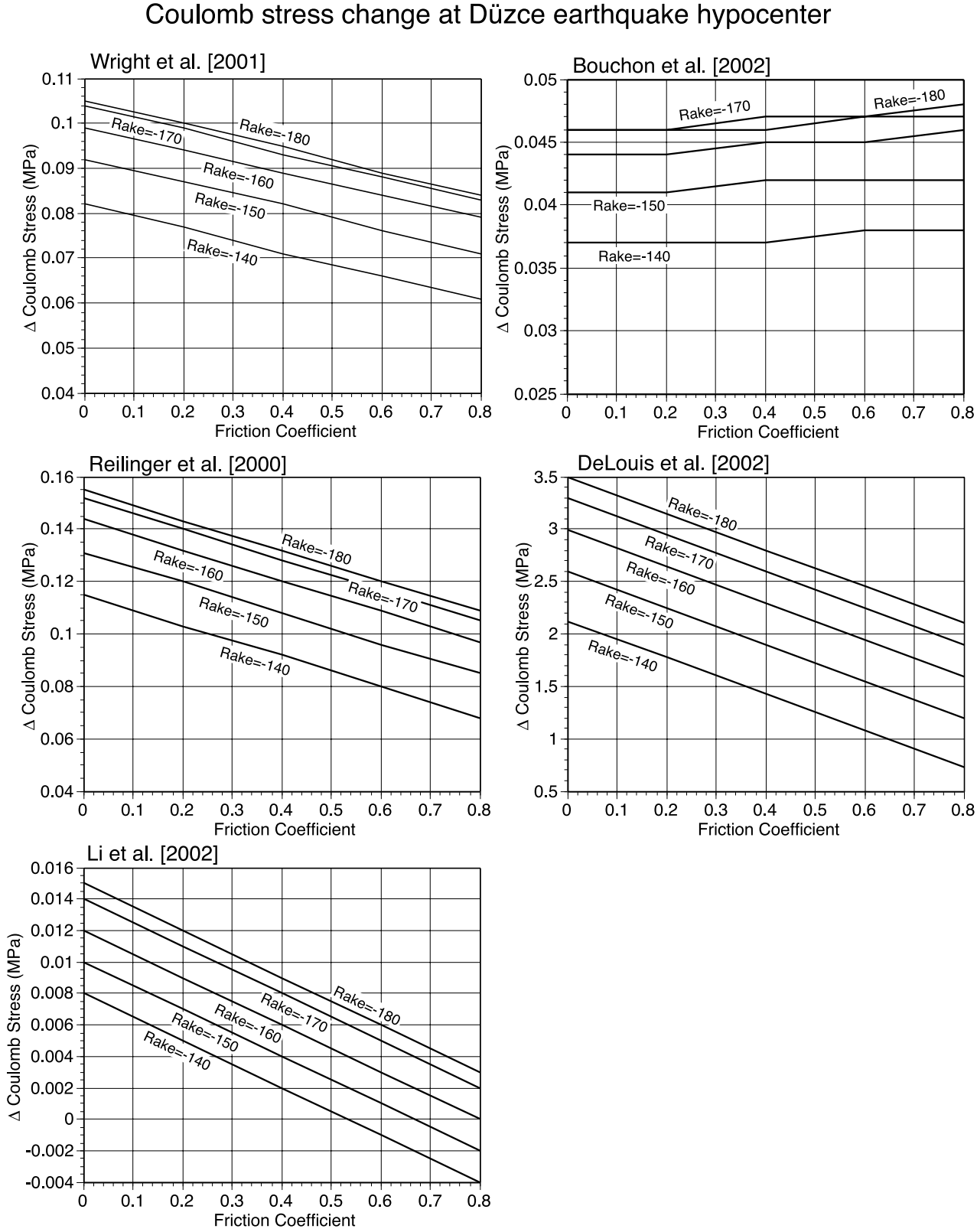

Figure 11. Variability of calculated Coulomb stress change at the hypocenter of the 12 November 1999 $M = 7.2$ Düzce earthquake hypocenter resulting from fault rakes ranging from $-140°$ to $-180°$, friction coefficients from 0 to 0.8, and five different Izmit earthquake slip models.

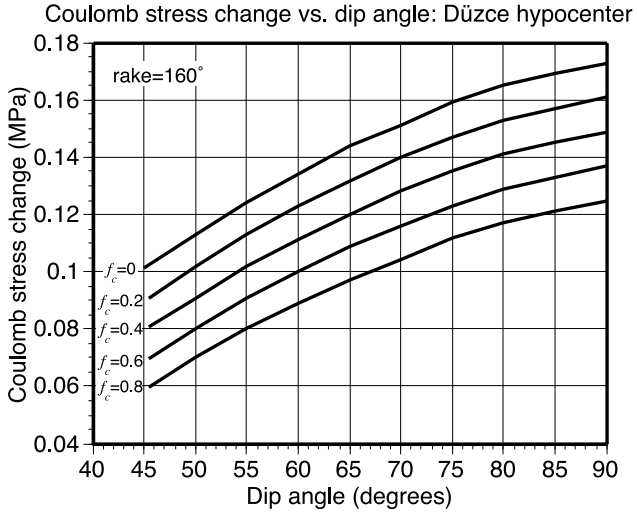

Figure 12. Variability in calculated Coulomb stress change at the Düzce hypocenter with dip angle and friction coefficient. Calculations in this example were made with the *Reilinger et al.* [2000] Izmit slip model.

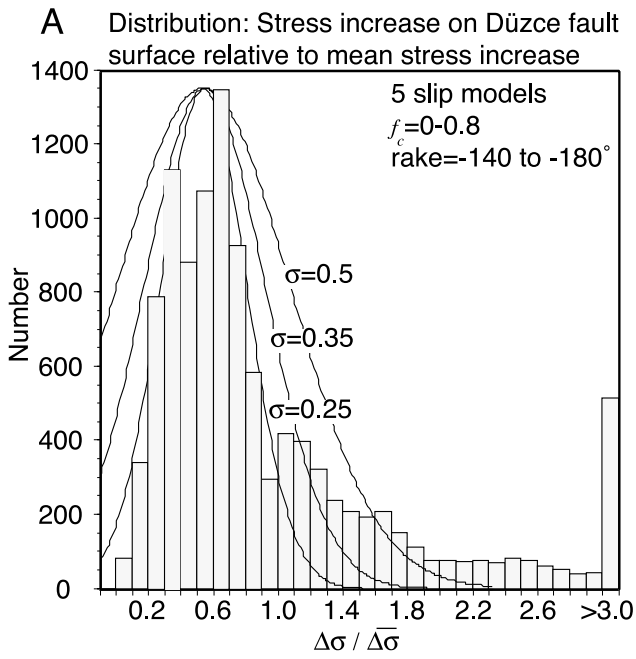

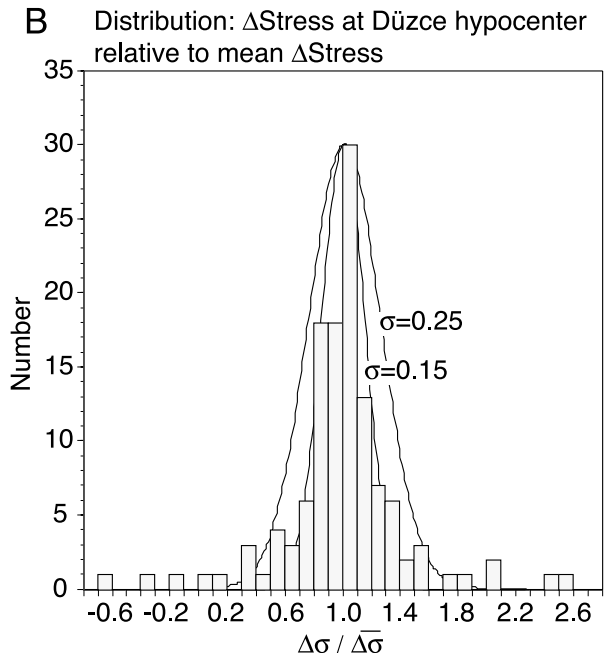

Figure 13. (a) Calculated distribution of increased stress ($\Delta\sigma > 0.01$ MPa) patches (2.5 × 0.5 km) on the Düzce fault plotted relative to the mean of all stress-increased patches. The distribution includes calculations from five different slip models and a range of friction coefficients and rakes. The majority of stress-increased fault patches are approximately normally distributed between the mean and zero; three sample normal distributions are plotted with standard deviations between 0.25 and 0.5. (b) Distribution of calculated Coulomb stress changes at the Düzce hypocenter plotted relative to the mean for the same range of slip models, rakes, and friction coefficients as in Figure 13a.

treat a stress change as an advance or delay in the earthquake cycle. Under the renewal model, fault stress builds with time because of tectonic plate motion. Thus a sudden stress change should be equivalent to a sudden shift in the time to the next earthquake. The advance or delay (clock change T') can be estimated by dividing the stress change (ΔCF) by the tectonic stressing rate ($\dot{\tau}$), as $T' = \Delta CF/\dot{\tau}$. Probability is accrued from the last earthquake time adjusted by the clock change ($T_0 + T'$) [e.g., *Working Group on California Earthquake Probabilities* (*WGCEP*), 1990]. Alternatively, the earthquake interevent time μ can be adjusted by the clock change as $\mu = \mu_0 + T'$.

[33] The choice of whether to change the elapsed time or the interevent time has a potentially significant effect on the resulting earthquake probability calculation. Probability calculated with a clock change, or elapsed time shift, is most significant at the time of the stress change, and then asymptotes to the maximum probability value with time (Figure 15). A change in recurrence interval has the opposite characteristic. The probability change is smallest at the time of the stress change, and then asymptotes to a permanent offset in probability (Figure 15). These differences are caused because in one instance (recurrence interval change), the mean of the recurrence distribution is changed and thus the maximum calculated probability changes. In the case where the last earthquake time is changed (clock change), the center of the distribution is unaffected; thus, after a long elapsed time, the maximum calculated probability stays the same.

[34] These differences could be important for cases like the interaction between the 1906 San Francisco earthquake and the north Hayward fault shown in Figure 15, where nearly 100 years have passed since the stress change; is there still an effect on the probability of Hayward fault earthquakes? Unfortunately, there is no clear justification for choosing one method over the other, and the differences

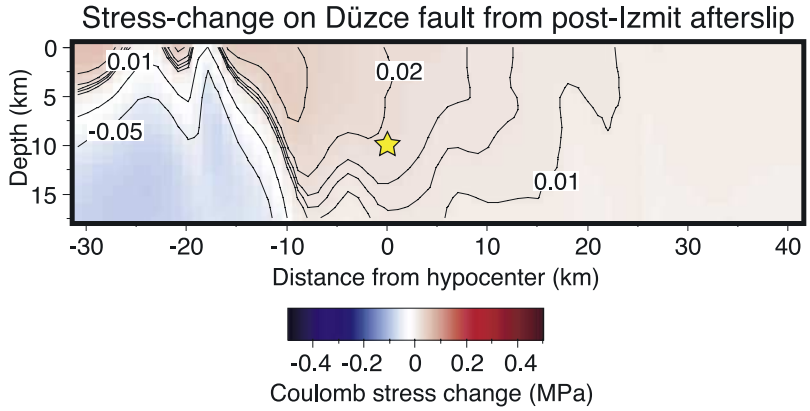

Figure 14. Calculated Coulomb stress change on the Düzce fault plane from modeled postseismic deformation following the Izmit earthquake [*Bürgmann et al.*, 2002], using a friction coefficient of 0.2 and a rake of −160°.

must be considered as part of the variability associated with interaction probability calculations.

4.2. Tectonic Loading Rate

[35] Making a clock change or interevent time adjustment in probability calculations requires an estimate of the tectonic stressing rate. Different techniques for stressing rate calculations result in very different assumptions about the distribution of lithospheric stress. A commonly used approach to estimating tectonic loading is to simulate the earthquake fault as a dislocation; the seismogenic part of the fault is locked while the rest of the fault is allowed to slip freely. This type of model assumes that almost all crustal stress is concentrated on faults, while almost none is found in the crust as a whole (Figure 16). In contrast, solid three-dimensional (3-D) models of crustal deformation tend to have a more uniform crustal stress distribution (Figure 16). Dislocation models will indicate much higher tectonic loading rates, leading to smaller clock or interevent time changes for a given stress change calculation, hence smaller probability changes [e.g., *Parsons*, 2002b, 2004].

4.3. Transient Probability Change

[36] A transient change in seismicity rate following an earthquake is a long recognized [*Omori*, 1894; *Dutton*, 1904], widely observed phenomenon. The physics of the process [e.g., *Scholz*, 1968; *Dieterich*, 1994; *Marcellini*, 1997; *Kilb et al.*, 2002; *Felzer et al.*, 2003] and how to work it into earthquake probability calculations [e.g., *Dieterich and Kilgore*, 1996; *Matthews et al.*, 2002; *Hardebeck*, 2004; J. Gomberg et al., unpublished data, 2004] are still debated. Much like the overall question whether to incorporate stress transfer into time-dependent earthquake probability calculations, the issue whether to fold in transient seismicity rate changes pits observational evidence against the uncertainty and variability of probability calculations. At present, three methods for transient probability change calculations are in use; two techniques from rate state friction theory [*Dieterich and Kilgore*, 1996; *Toda et al.*, 1998; *Hardebeck*, 2004], and one from the Brownian passage time model [*Matthews et al.*, 2002; *WGCEP*, 2003].

4.3.1. Rate State Transient

[37] The rate state transient effect describes an expected enhanced rate of earthquake nucleation resulting from a stress increase, and can be expressed as a probability. For a stress decrease, the rate of nucleation declines, and eventually recovers. *Dieterich* [1994] derived a time-

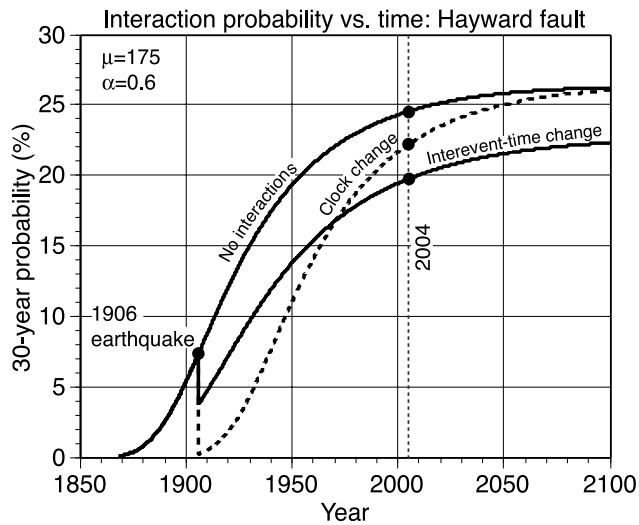

Figure 15. Thirty-year conditional probability versus time on the Hayward fault in northern California after a calculated 0.5-MPa stress decrease associated with the 1906 M = 7.9 San Francisco earthquake. Interaction probability calculations were made with (1) a clock change, where the time of the last earthquake was set forward an amount proportional to the stress change, and (2) with an interevent time change, where the interevent time was lengthened by an amount proportional to the stress change. The two methods generate different probability values at different times in the earthquake cycle.

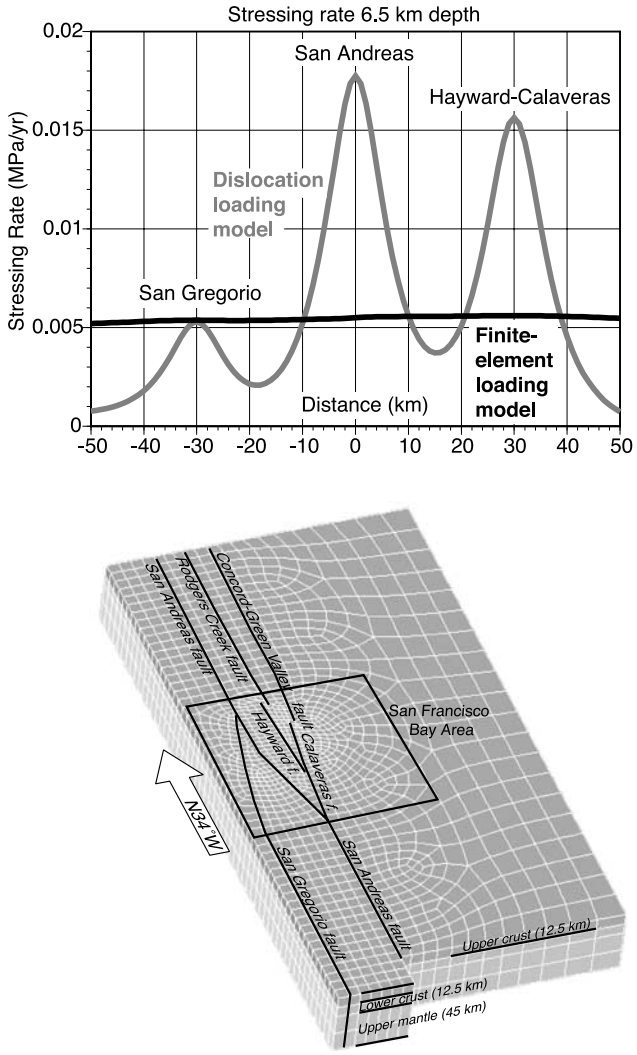

Figure 16. Example tectonic stressing rate calculations for the San Francisco Bay region [*Parsons*, 2002b]. (a) Stressing rate plotted at 6 km depth on a profile orthogonal to the relative plate motion vector. Black line results from the 3-D finite element model shown in Figure 16b. Gray line is calculated from a deep dislocation model. This plot illustrates variability in clock change adjustments for probability calculations because these are usually calculated by dividing Coulomb stress change by a loading rate value.

dependent seismicity rate $R(t)$, after a stress perturbation as

$$R(t) = \frac{r}{[\exp(-\Delta\tau/a\sigma) - 1]\exp[-t/t_a] + 1} \quad (5)$$

where r is the steady state seismicity rate, $\Delta\tau$ is the stress step, σ is the normal stress, a is a fault constitutive constant, and t_a is an observed aftershock duration, a fault-specific parameter.

[38] The transient change in expected earthquake rate $R(t)$ after a stress step can be related to the probability of an earthquake of a given size over the time interval Δt through a nonstationary Poisson process as

$$P(t, \Delta t) = 1 - \exp\left[-\int_t^{t+\Delta t} R(t)dt\right] = 1 - \exp[-N(t)], \quad (6)$$

after *Dieterich and Kilgore* [1996], where $N(t)$ is the expected number of earthquakes in the interval Δt. This transient probability change is superimposed on the permanent change that results from a time shift, or a change in the repeat time as discussed previously. Integrating for $N(t)$ yields

$$N(t) = r_p\left\{\Delta t + t_a \ln\left[\frac{1 + [\exp(-\Delta\tau/a\sigma) - 1]\exp[-\Delta t/t_a]}{\exp(-\Delta\tau/a\sigma)}\right]\right\} \quad (7)$$

where r_p is the expected rate of earthquakes associated with the permanent probability change [*Toda et al.*, 1998]. This rate can be determined by again applying a stationary Poisson probability expression as

$$r_p = \left(\frac{-1}{\Delta t}\right)\ln(1 - P_c) \quad (8)$$

where P_c is a conditional probability, and can be calculated using any distribution.

[39] There are advantages in using the rate state model, though a number of important assumptions must also be made. Rate state friction laws describe physical processes that govern rock friction behavior in the laboratory setting. Most of the assumptions evolve from extrapolation to natural faults, and from presupposing stress conditions and distributions on natural faults. Under the *Dieterich* [1994] model, a group of faults or even a single fault is considered an infinite population of earthquake nucleation sites that are near to failure. These conditions are treated as Poissonian [*Dieterich and Kilgore*, 1996], are independent of the fault rupture history, and are applied on top of the static probability change.

[40] *Hardebeck* [2004] suggests that superimposing the transient response onto a clock change, or static probability change is double counting, and proposes a method to calculate interaction probabilities that uses time-varying clock change corrections. Integration limits of a probability density function are changed with each time step to simulate a variety of potential earthquake nucleation sites. If a rate state nucleation model [*Dieterich*, 1994] is implemented, as [*Hardebeck*, 2004]

$$T_{old} = \frac{A\sigma}{\dot{\tau}}\ln\left[\left(\exp\left(\frac{T_{new}\dot{\tau}}{A\sigma}\right) - 1\right)\exp\left(\frac{\Delta\tau}{A\sigma}\right) + 1\right], \quad (9)$$

then a transient response in probability change is obtained (Figure 17). The probability that nucleation will occur between the new limits is calculated using the original density function.

[41] Comparison of the two rate state methods shows a similar shape in the evolution of probability with time; a higher peak is obtained with the time-varying clock change method [*Hardebeck*, 2004] than with the *Dieterich and Kilgore* [1996] method (Figure 17). Rate state parameters used in both instances imply an aftershock decay time of 10 years, and by 20–30 years after the stress step, the probability changes are equivalent.

4.3.2. Brownian Passage Time

[42] A sudden stress change, or state change in Brownian terms, can produce a transient probability change depending

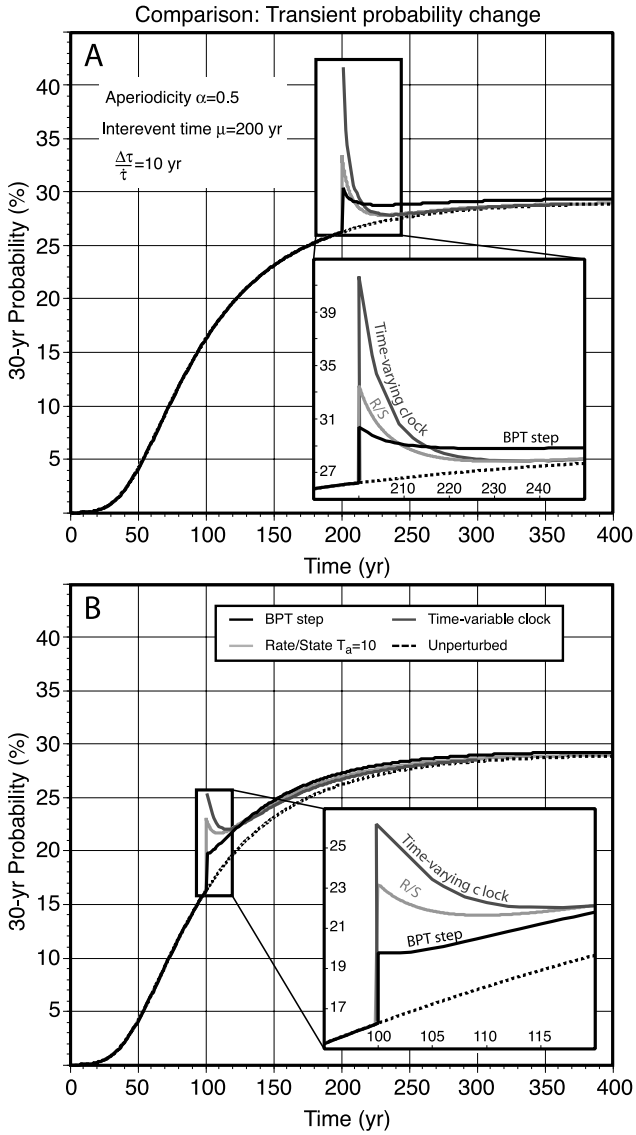

Figure 17. Comparison of three different implementations of transient probability changes resulting from sudden stress changes. (a) A 0.1 MPa stress change applied 200 years into a 200-year earthquake cycle. A sharp increase in probability is calculated (using a Brownian distribution) with all methods; the time-varying clock change method of *Hardebeck* [2004] shows the largest change, the rate state technique of *Dieterich and Kilgore* [1996] is intermediate, and the Brownian passage time step model of *Matthews et al.* [2002] has the smallest change. (b) Same stress step but applied at 100 years into the cycle. In all three cases the transient is less pronounced than in Figure 17a.

upon time elapsed since the last earthquake [*Matthews et al.*, 2002]. The transient results from an entirely different origin than in the rate state models. Aperiodicity in the Brownian model comes from random noise superimposed on a state evolution function. Following a stress step late in the cycle, a sudden increase in state has a relatively high probability of causing failure, which leads to a spike in calculated probability (Figure 17). However, continuous random fluctuations in state cause the spike in probability to approach the background rate over time, which produces a decaying transient probability change [*Matthews et al.*, 2002].

[43] The calculated spike in probability from a stress step using the Brownian model is less pronounced than those calculated with the rate state methods (Figure 17), especially for a step earlier in the cycle (Figure 17b). However, the duration of the probability change is longer lived, resembling an interevent time adjustment more than a clock change (Figure 15).

4.3.3. Variability Introduced by Different Transient Calculation Methods

[44] Global observations indicate that the duration of transient seismicity rate increase following a stress step is between ~7–12 years [e.g., *Kagan*, 1994; *Dieterich*, 1994; *Parsons*, 2002a]. Indeed, in the examples shown in Figure 17, the important variability between the methods is confined within the decade following the stress step and is largest in the first year or two. Depending upon the method applied, input parameters, and timing of the stress step (Figure 17b), variation among the methods can exceed 10% for a short time. Unfortunately, there is not a good way to calibrate the peak of the transient against data. Thus, if probability is calculated shortly after a stress perturbation, and it is desired to capture the transient response, a large degree of uncertainty must be accommodated.

5. How Large Must a Stress Change be to Cause a Meaningful Probability Change?

[45] Clearly, there is significant uncertainty in collecting parameters to make an interaction probability calculation. Drawing from paleoseismic and historical earthquake catalogs allows for many viable interevent models, making stress change calculations adds another layer of variability, and choices must be made as to how to assimilate them as probability changes. These choices are to some extent uninformed by data, and decisions are often made on a philosophical basis. The logic applied here is to ask at what point does the signal of a stress change become large enough such that all the other variability becomes less important by comparison? The example pursued here is from the interaction between the 1992 M = 7.4 Landers earthquake and the adjacent San Andreas fault in southern California. This choice is made because variability associated with the paleoseismic catalogs on the San Andreas has already been explored in this paper, the Landers event is well studied, and *Hardebeck* [2004] also calculated post-Landers San Andreas fault probability changes. The calculated stress change from the Landers event is characterized as a distribution relative to the mean stress change (Figure 18), but the magnitude of the mean stress change is scalable in this example to investigate how large it must be to cause a significant perturbation in calculated probability. In other words, the shape of the stress change pattern is preserved, but its amplitude can be changed. In this way the results are made more general beyond the San Andreas case.

[46] The Landers earthquake occurred between ~40 to ~100 km from the San Andreas fault, and is calculated to have caused a heterogeneous stress change (Figure 18), with large areas of positive and negative Coulomb stress

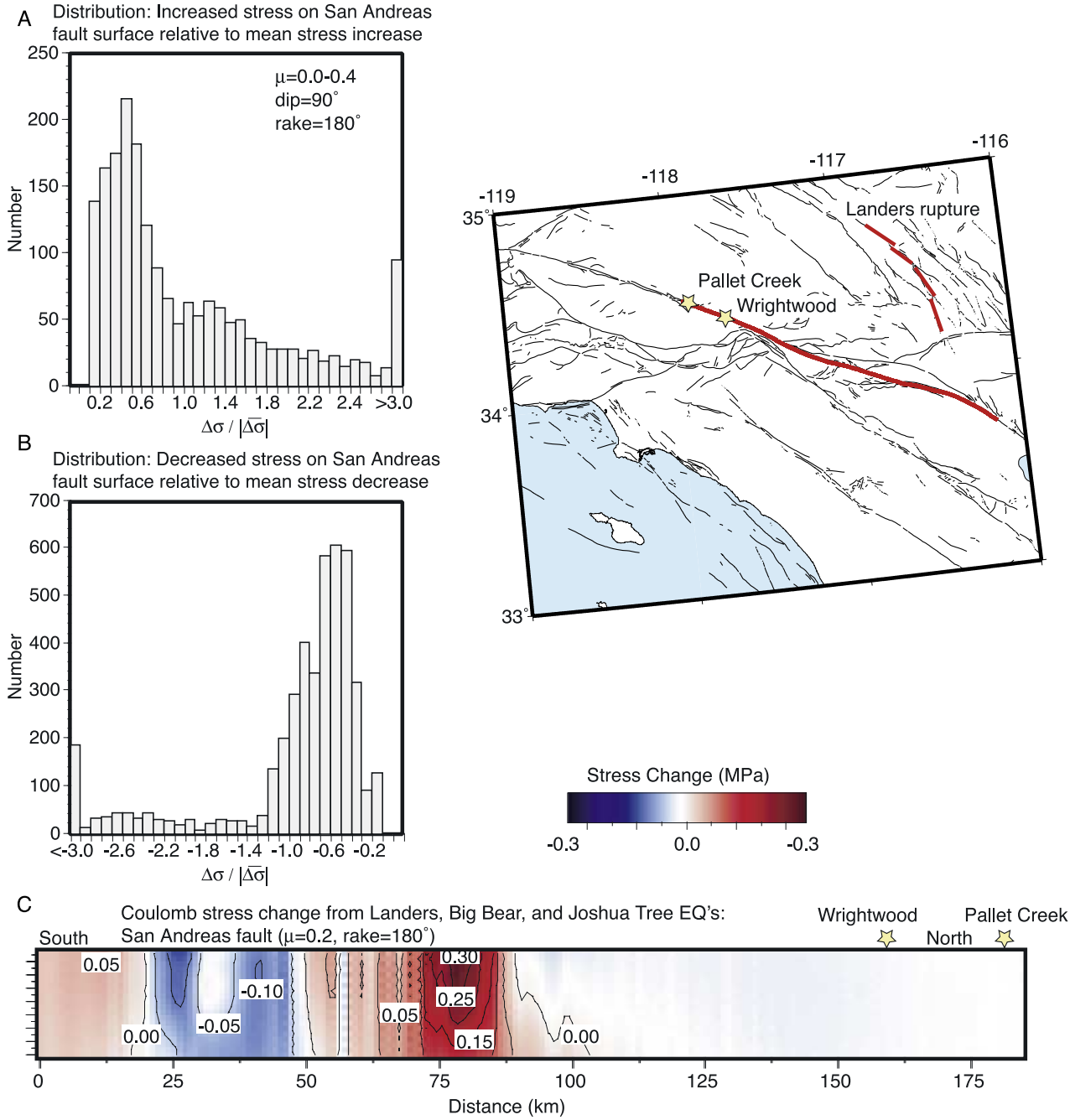

Figure 18. Landers earthquake effects on the San Andreas fault in southern California. (a) Distribution of calculated increased stress ($\Delta\sigma > 0.01$ MPa) patches (1 × 2 km) on the San Andreas fault plotted relative to the mean of all stress-increased patches on the segment. Values calculated over a range of friction coefficients from 0 to 0.4 are included. (b) Distribution of calculated decreased stress patches on the San Andreas fault. (c) Contour plot of calculated stress changes using a friction coefficient of 0.2.

change. Calculations were made for a range of friction coefficients between $f_c = 0$ and $f_c = 0.4$ as determined from analysis of microseismicity before and after the Landers event [*Parsons et al.*, 1999]. The San Andreas fault is assumed vertical with a strike-slip rake of 180°. Coulomb stress changes were calculated with the slip model of *Wald and Heaton* [1994], and changes of absolute value greater than 0.01 MPa were included in the analysis.

[47] San Andreas fault patches (~1 × 2 km) with calculated stress increase and decrease have a similar distribution relative to mean stress change (Figure 18) as calculated for the Izmit effect on the Düzce fault (Figure 13), with most of the patches approximately normally distributed between 0 and the mean. Stress change values were drawn at random from the stress-increased distribution with the mean scaled by different amounts, expressed as a ratio of the mean stress change and tectonic stressing rate (clock change). Ratios

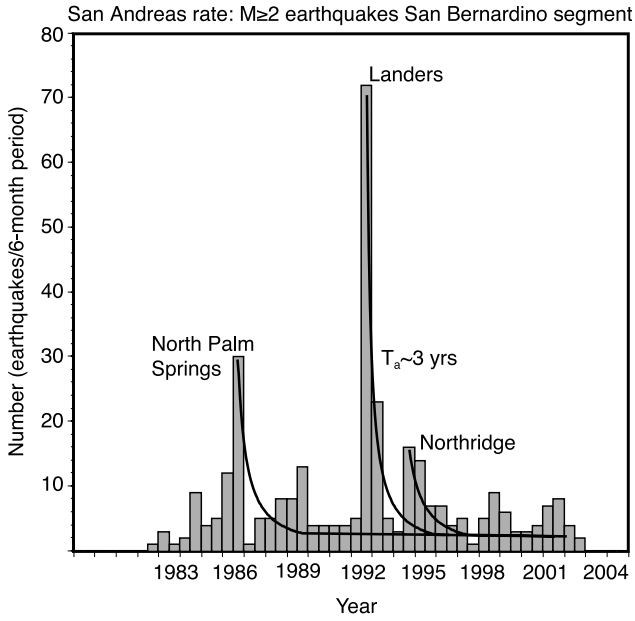

Figure 19. Seismicity rate changes within ±1 km of the San Andreas fault (trace shown in Figure 18). The aftershock durations from three earthquakes are shown. In all cases the rate returns to background within ~3 years.

from 10 to 50 were explored, which are the equivalent of a 0.1 to 0.5 MPa stress change relative to a typical San Andreas fault stressing rate of ~0.01 MPa/yr [*Parsons*, 2002b]. Stress change values were used to perturb the distribution of probabilities calculated from the permissible San Andreas fault interevent models that fit the Wrightwood paleoseismic and historic catalog (Figure 1). Three methods for incorporating the stress changes into time-dependent probabilities were compared: (1) the rate state method of *Dieterich and Kilgore* [1996] and *Toda et al.* [1998] superimposed on a clock change, (2) the time-varying clock change method developed by *Hardebeck* [2004] using a rate state nucleation model, and (3) the Brownian passage time step model [*Matthews et al.*, 2002]. In all cases the Brownian distribution of equation (3) was used to accrue 30-year conditional probability for the year 2004.

[48] Needed parameters for the interaction probability calculations are: (1) the set of interevent-aperiodicity pairs from the earthquake catalog, (2) for each interevent time-aperiodicity pair, a set of 100 scaled clock change values (mean clock change between 10 and 50) drawn from the Landers stress change distribution, and (3) for the rate state transient probability calculations, an estimate of the aftershock decay rate on the San Andreas fault. The seismicity rate of $M \geq 2$ earthquakes that occurred within 1 km of the San Andreas fault plane is shown in Figure 19. The effects of three large earthquakes are evident, with seismicity spikes following the 1986 M = 5.6 North Palm Springs, 1992 M = 7.4 Landers, and 1994 M = 6.7 Northridge earthquakes. In all three instances, seismicity rates are not distinguishable from the background rate after ~3 years; thus rate state parameters consistent with a 3-year aftershock decay rate are derived for the calculations (see section 4.3.1 for details).

[49] After the stress change perturbations were applied, distributions of probability values were compared with the unperturbed, and differences analyzed for significance. The approach taken differs from that of *Hardebeck* [2004], who assumed a significance measure of one standard deviation of probability change above the mean of many calculations; here I look for significant skew in the array of answers, which are typically not normally distributed. The probability distributions were compared using a Kolmogoroff-Smirnoff test, which is sensitive to distribution shapes, particularly the mean, median, dispersion, and skewness [e.g., *Sachs*, 1982]. The test statistic

$$\hat{D} = \max\left|\left(\frac{F_1}{n_1} - \frac{F_2}{n_2}\right)\right|, \tag{10}$$

where F_1 and F_2 are cumulative frequencies, and n_1 and n_2 are sample sizes, is compared to the critical value

$$D_{(\alpha)} = K_{(\alpha)}\sqrt{\frac{n_1 + n_2}{n_1 n_2}}, \tag{11}$$

where $K_{(\alpha)}$ is a constant reflecting the level of significance. If $\hat{D} < D_{(\alpha)}$, then there is no demonstrable difference between the two distributions at a given confidence level.

[50] In the first series of tests, stress change values were drawn from the whole distribution of increases shown in Figure 18, and multiplied by scales from 10 to 50, to get clock change values meant to cover a reasonable range of about 0.1 to 0.5 MPa stress changes relative to a ~0.01 MPa/yr stressing rate. However, even when scaled by 50, no significant difference between the unperturbed and perturbed set of probability values could be established above 80% confidence level as measured with the Kolmogoroff-Smirnoff test. In a second set of tests, only stress changes above the mean were used, and values scaled by factors between 10 and 50 did cause significant changes to the distribution of probability values (Figure 20).

[51] Significant changes (80–90% confidence) to the range of post-Landers probability on the San Andreas fault were noted using the *Dieterich and Kilgore* [1996] method to perturb probability when the mean of the stress change distribution was scaled by a factor of 20 or greater (Figure 20a). The short aftershock duration observed for the San Andreas fault (Figure 19) means that most of the rate state transient probability increase calculated from the 1992 Landers earthquake stress changes has extinguished by the beginning of the 2004 calculation interval, and the perturbations are much like a standard clock change calculation. The duration of the Brownian step transient calculation tends to be longer (Figure 17). Thus the same clock changes applied cause more significant probability changes (Figure 20b), ranging from 85% confidence when scaled by a factor of 10, to 99% when scaled by 50. In contrast, the time-varying clock change method of *Hardebeck* [2004] has no permanent probability change associated with stress changes. Thus, in 2004, 12 years after the Landers earthquake, no significant change in probability is noted with that method regardless of the magnitude of stress change (Figure 20c).

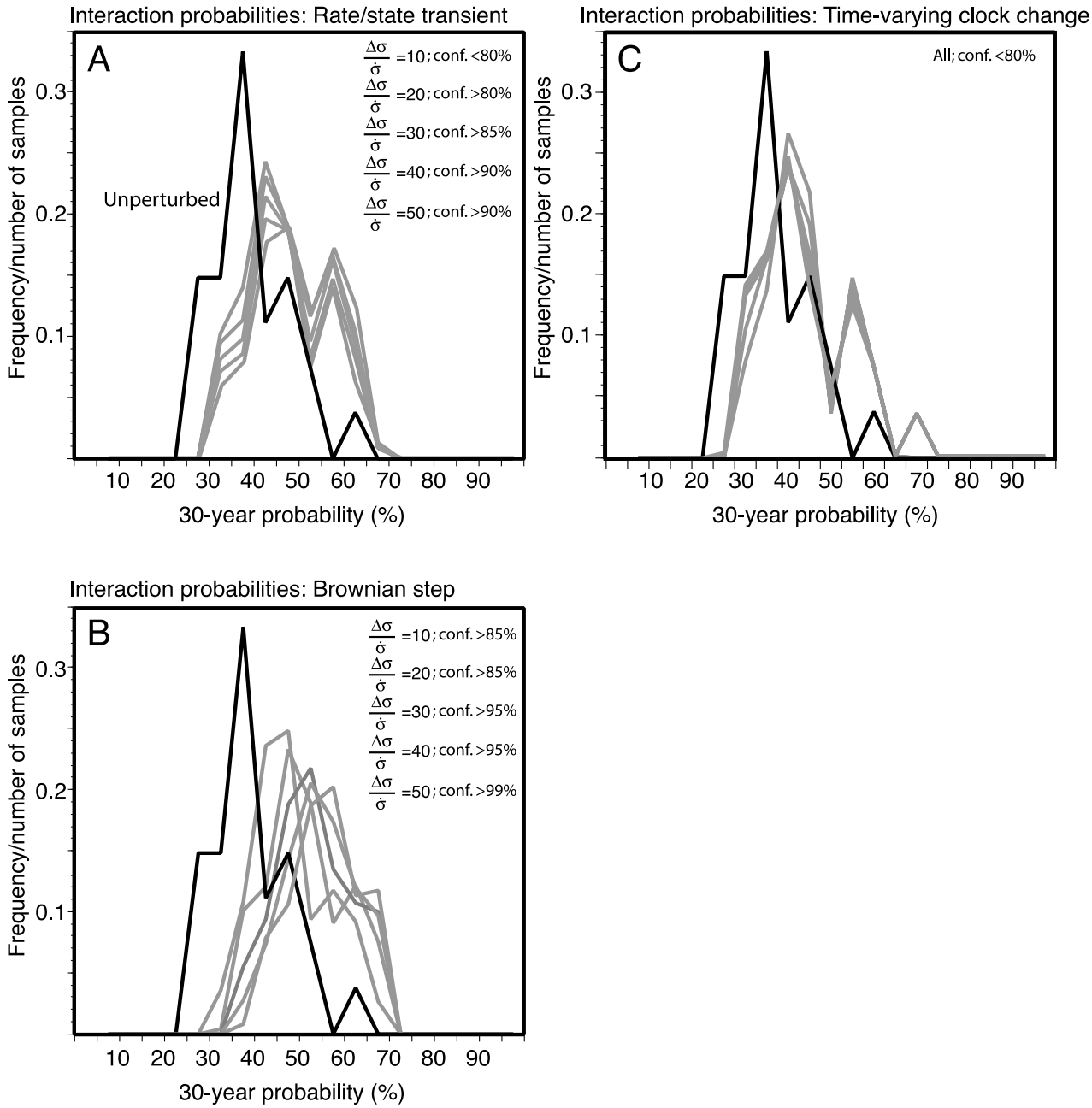

Figure 20. Perturbations of probability on the southern San Andreas fault using the Wrightwood interevent time and aperiodicity pairs from Figure 1 and drawing at random from the distribution of increased stress (greater than the mean increase) shown in Figure 18a. Changes to probability distributions are shown for clock change scales ranging from 10 to 50 for three different calculation methods: (a) the rate state method of *Dieterich and Kilgore* [1996], (b) the Brownian passage time step model of *Matthews et al.* [2002], and (c) the time-variable clock change with rate state nucleation method of *Hardebeck* [2004].

[52] In summary, the results of the Landers-San Andreas test indicate that, for a fault segment well-characterized by paleoseismic observations, probability changes might best be calculated in areas where the stress is changed in excess of the segment mean. Depending on the probability calculation technique used, mean stress change on a fault segment needs to be at least 10–20 times greater than the tectonic stressing rate for probability changes to be significant. This means that the perturbed fault must be quite close to the earthquake rupture as in the case of the Izmit-Düzce pair, or the tectonic stressing rate must be very low.

6. Conclusions

[53] An earthquake history that is well characterized by paleoseismic and historical observations can be fit with a broad range of interevent time and aperiodicity models, all

with about equal chance of being correct. Thus earthquake probability may best be expressed as a range of acceptable answers [*Savage*, 1991, 1992]. Modeling of stress transfer and tectonic stressing carries significant uncertainty. Additionally, different methods of integrating a sudden change in fault stress in probability calculations give an array of different answers. Nonetheless, incorporation of stress transfer in earthquake probability calculations can be justified in circumstances where the calculated stress change on a fault is at least 10–20 times greater than the calculated tectonic stressing rate. In practical terms, this would be a large earthquake or other stress perturbation happening closer than a few tens of kilometers from a fault zone of well-documented earthquake history that is loaded at a moderate rate. In such cases, the range of probability values is calculated to be altered with a high degree of confidence.

[54] **Acknowledgments.** Improvements to this manuscript were made because of reviews by Ned Field, Mark Stirling, and Associate Editor Sandy Steacy. Paul Reasenberg provided source code for the Brownian passage time step interaction probability calculations, and Jeanne Hardebeck provided her algorithm for translating stress changes into probability changes. Bob Simpson provided and supported his DLC code for making stress transfer calculations. I thank Michel Bouchon, Roland Bürgmann, Bertrand De Louis, Xu Li, Haruko Sekiguchi, and Tim Wright for sharing their Izmit earthquake source models.

References

Ambraseys, N. N. (2002), The seismic activity of the Marmara Sea region over the last 2000 years, *Bull. Seismol. Soc. Am.*, *92*, 1–18.

Anderson, G., B. Aagaard, and K. Hudnut (2003), Fault interactions and large complex earthquakes in the Los Angeles area, *Science*, *302*, 1946–1949.

Bakun, W. H. (1999), Seismic activity of the San Francisco Bay region, *Bull. Seismol. Soc. Am.*, *89*, 764–784.

Bakun, W. H., and C. M. Wentworth (1997), Estimating earthquake location and magnitude from seismic intensity data, *Bull. Seismol. Soc. Am.*, *87*, 1502–1521.

Beeler, N. M., R. W. Simpson, S. H. Hickman, and D. A. Lockner (2000), Pore fluid pressure, apparent friction, and Coulomb failure, *J. Geophys. Res.*, *105*, 25,533–25,542.

Belardinelli, M. E., M. Cocco, O. Coutant, and F. Cotton (1999), Redistribution of dynamic stress during coseismic ruptures: Evidence for fault interaction and earthquake triggering, *J. Geophys. Res.*, *104*, 14,925–14,945.

Biasi, G. P., R. J. Weldon II, T. E. Fumal, and G. G. Seitz (2002), Paleoseismic event dating and the conditional probability of large earthquakes on the southern San Andreas fault, California, *Bull. Seismol. Soc. Am.*, *92*, 2761–2781.

Bouchon, M., M. N. Toksoz, H. Karabulut, M.-P. Bouin, M. Dietrich, M. Aktar, and M. Edie (2002), Space and time evolution of rupture and faulting during the 1999 Izmit (Turkey) earthquake, *Bull. Seismol. Soc. Am.*, *92*, 256–266.

Bürgmann, R., S. Ergintav, P. Segall, E. H. Hearn, S. C. McClusky, R. E. Reilinger, H. Woith, and J. Zschau (2002), Time-dependent distributed afterslip on and deep below the Izmit earthquake rupture, *Bull. Seismol. Soc. Am.*, *92*, 1450–1469.

Delouis, B., D. Giardini, P. Lundgren, and J. Salichon (2002), Joint inversion of InSAR, GPS, teleseismic, and strong-motion data for the spatial and temporal distribution of earthquake slip: Application to the 1999 Izmit mainshock, *Bull. Seismol. Soc. Am.*, *92*, 278–299.

Dieterich, J. H. (1994), A constitutive law for rate of earthquake production and its application to earthquake clustering, *J. Geophys. Res.*, *99*, 2601–2618.

Dieterich, J. H., and B. Kilgore (1996), Implications of fault constitutive properties for earthquake prediction, *Proc. Natl. Acad. Sci. U.S.A.*, *93*, 3787–3794.

Dutton, C. E. (1904), *Earthquakes in the Light of the New Seismology*, 314 pp., Penguin USA, East Rutherford, N. J.

Ellsworth, W. L. (1990), Earthquake history, 1769–1989, in *The San Andreas Fault System*, edited by R. E. Wallace, *U. S. Geol. Surv. Prof. Pap.*, *1515*, 153–187.

Felzer, K. R., R. E. Abercrombie, and G. Ekström (2003), Secondary aftershocks and their importance for aftershock forecasting, *Bull. Seismol. Soc. Am.*, *93*, 1433–1448.

Fumal, T. E., R. J. Weldon II, G. P. Biasi, T. E. Daeson, G. G. Seitz, W. T. Frost, and D. P. Schwartz (2002), Evidence for large earthquakes on the San Andreas fault at the Wrightwood, California, Paleoseismic site: A.D. 500 to present, *Bull. Seismol. Soc. Am.*, *92*, 2726–2760.

Gomberg, J., P. Bodin, and P. A. Reasenberg (2003), Observing earthquakes triggered in the near field by dynamic deformations, *Bull. Seismol. Soc. Am.*, *93*, 118–138.

Hagiwara, Y. (1974), Probability of earthquake occurrence as obtained from a Weibull distribution analysis of crustal strain, *Tectonophysics*, *23*, 318–323.

Hardebeck, J. L. (2004), Stress triggering and earthquake probability estimates, *J. Geophys. Res.*, *109*, B04310, doi:10.1029/2003JB002437.

Harris, R. A. (1998), Introduction to special section: stress triggers, stress shadows, and implications for seismic hazard, *J. Geophys. Res.*, *103*, 24,347–24,358.

Harris, R. A., and R. W. Simpson (1998), Suppression of large earthquakes by stress shadows: A comparison of Coulomb and rate-and-state failure, *J. Geophys. Res.*, *103*, 24,439–24,452.

Hearn, E. H., R. Bürgmann, and R. E. Reilinger (2002), Dynamics of Izmit earthquake postseismic deformation and loading of the Düzce earthquake hypocenter, *Bull. Seismol. Soc. Am.*, *92*, 172–193.

Hubert-Ferrari, A., A. Barka, E. Jaques, S. S. Nalbant, B. Meyer, R. Armijo, P. Tapponnier, and G. C. P. King (2000), Seismic hazard in the Marmara Sea region following the 17 August 1999 Izmit earthquake, *Nature*, *404*, 269–273.

Ishibashi, K., and K. Satake (1998), Problems on forecasting great earthquakes in the subduction zones around Japan by means of paleoseismology, *J. Seismol. Jpn.*, *50*, 1–21.

Kagan, Y. Y. (1994), Incremental stress and earthquakes, *Geophys. J. Int.*, *117*, 345–364.

Kagan, Y. Y., and L. Knopoff (1987), Random stress and earthquake statistics: time dependence, *Geophys. J. R. Astron. Soc.*, *88*, 723–731.

Kilb, D., J. S. Gomberg, and P. Bodin (2000), Triggering of earthquake aftershocks by dynamic stresses, *Nature*, *408*, 570–574.

Kilb, D., J. Gomberg, and P. Bodin (2002), Aftershock triggering by complete Coulomb stress changes, *J. Geophys. Res.*, *107*(B4), 2060, doi:10.1029/2001JB000202.

Li, X., V. F. Cormier, and M. N. Toksoz (2002), Complex source process of the 17 August 1999 Izmit, Turkey, earthquake, *Bull. Seismol. Soc. Am.*, *92*, 267–277.

Lienkaemper, J. J., T. E. Dawson, S. F. Personius, G. G. Seitz, Liam M. Reidy, and D. P. Schwartz (2002), A record of large earthquakes on the southern Hayward fault for the past 500 years, *Bull. Seismol. Soc. Am.*, *92*, 2637–2658.

Lienkaemper, J., P. Williams, T. Dawson, S. Personius, G. Seitz, S. Heller, and D. Schwartz (2003), Logs and data from trenches across the Hayward Fault at Tyson's Lagoon (Tule Pond), Fremont, Alameda County, California, *U.S. Geol. Surv. Open File Rep.*, *03-488*, 6 pp., 8 plates. (available at http://geopubs.wr.usgs.gov/open-file/of03-488/)

Lu, C., D. Harte, and M. Bebbington (1999), A linked stress release model for historical Japanese earthquakes: Coupling among major seismic regions, *Earth Planets Space*, *51*, 907–916.

Marcellini, A. (1997), Physical model of aftershock temporal behavior, *Tectonophysics*, *277*, 137–146.

Matthews, M. V., W. L. Ellsworth, and P. A. Reasenberg (2002), A Brownian model for recurrent earthquakes, *Bull. Seismol. Soc. Am.*, *92*, 2233–2250.

Nishenko, S. P., and R. Buland (1987), A generic recurrence interval distribution for earthquake forecasting, *Bull. Seismol. Soc. Am.*, *77*, 1382–1399.

Nur, A., and G. Mavko (1974), Postseismic viscoelastic rebound, *Science*, *183*, 204–206.

Ogata, Y. (1999), Estimating the hazard of rupture using uncertain occurrence times of paleoearthquakes, *J. Geophys. Res.*, *104*, 17,995–18,014.

Okada, Y. (1992), Internal deformation due to shear and tensile faults in a half-space, *Bull. Seismol. Soc. Am.*, *82*, 1018–1040.

Omori, F. (1894), On the aftershocks of earthquakes, *J. Coll. Jpn. Imp. Univ.*, *7*, 111–200.

Parsons, T. (2002a), Global Omori law decay of triggered earthquakes: Large aftershocks outside the classical aftershock zone, *J. Geophys. Res.*, *107*(B9), 2199, doi:10.1029/2001JB000646.

Parsons, T. (2002b), Post-1906 stress recovery of the San Andreas fault system calculated from three-dimensional finite element analysis, *J. Geophys. Res.*, *107*(B8), 2162, doi:10.1029/2001JB001051.

Parsons, T. (2004), Recalculated probability of $M \geq 7$ earthquakes beneath the Sea of Marmara, Turkey, *J. Geophys. Res.*, *109*, B05304, doi:10.1029/2003JB002667.

Parsons, T., R. S. Stein, R. W. Simpson, and P. A. Reasenberg (1999), Stress sensitivity of fault seismicity: a comparison between limited-offset oblique and major strike-slip faults, *J. Geophys. Res.*, *104*, 20,183–20,202.

Parsons, T., S. Toda, R. S. Stein, A. Barka, and J. H. Dieterich (2000), Heightened odds of large earthquakes near Istanbul: An interaction-based probability calculation, *Science*, *288*, 661–665.

Reasenberg, P. A., and R. W. Simpson (1992), Response of regional seismicity to the static stress change produced by the Loma Prieta earthquake, *Science*, *255*, 1687–1690.

Reilinger, R. E., et al. (2000), Coseismic and postseismic fault slip for the 17 August 1999, M = 7.5, Izmit, Turkey earthquake, *Science*, *289*, 1519–1524.

Sachs, L. (1982), *Applied Statistics*, 707 pp., Springer, New York.

Savage, J. C. (1991), Criticism of some forecasts of the National Earthquake Prediction Evaluation Council, *Bull. Seismol. Soc. Am.*, *81*, 862–881.

Savage, J. C. (1992), The uncertainty in earthquake conditional probabilities, *Geophys. Res. Lett.*, *19*, 709–712.

Savage, J. C., and W. H. Prescott (1978), Asthenospheric readjustment and the earthquake cycle, *J. Geophys. Res.*, *83*, 3369–3376.

Scholz, C. H. (1968), Microfractures, aftershocks, and seismicity, *Bull. Seismol. Soc. Am.*, *58*, 1117–1130.

Scholz, C. H. (1990), *The Mechanics of Earthquake Faulting*, 439 pp., Cambridge Univ. Press, New York.

Schwartz, D. P., G. Seitz, J. Lienkaemper, T. Dawson, S. Hecker, W. Lettis, and K. Kelson (2001), The Bay Area earthquake cycle: A paleoseismic perspective, *Eos Trans. AGU*, *82*(47), Fall Meet. Suppl., Abstract S12F-07.

Sieh, K., M. Stuiver, and D. Brillinger (1989), A more precise chronology of earthquakes produced by the San Andreas fault in southern California, *J. Geophys. Res.*, *94*, 603–623.

Steacy, S., D. Marsan, S. S. Nalbant, and J. McCloskey (2004), Sensitivity of static stress calculations to the earthquake slip distribution, *J. Geophys. Res.*, *109*, B04303, doi:10.1029/2002JB002365.

Stein, R. S., A. A. Barka, and J. H. Dieterich (1997), Progressive failure on the North Anatolian fault since 1939 by earthquake static stress triggering, *Geophys. J. Int.*, *128*, 594–604.

Toda, S., R. S. Stein, P. A. Reasenberg, J. H. Dieterich, and A. Yoshida (1998), Stress transferred by the 1995 M_w = 6.9 Kobe, Japan, shock: Effect on aftershocks and future earthquake probabilities, *J. Geophys. Res.*, *103*, 24,543–24,565.

Usami, T. (1988), Study of historical earthquakes in Japan, *Bull. Earthquake Res. Inst. Univ. Tokyo*, *54*, 399–439.

Wald, D. J., and T. H. Heaton (1994), Spatial and temporal distribution of slip for the 1992 Landers, California earthquake, *Bull. Seismol. Soc. Am.*, *84*, 668–691.

Working Group on California Earthquake Probabilities (WGCEP) (1990), Probabilities of large earthquakes in the San Francisco Bay region, California, *U. S. Geol. Surv. Circ.*, *1053*, 51 pp.

Working Group on California Earthquake Probabilities (WGCEP) (2003), Earthquake probabilities in the San Francisco Bay region: 2002 to 2031, *U.S. Geol. Surv. Open File Rep.*, *03-214*.

Wright, T., E. Fielding, and B. Parsons (2001), Triggered slip: observations of the 17 August 1999 Izmit (Turkey) earthquake using radar interferometry, *Geophys. Res. Lett.*, *28*, 1079–1082.

T. Parsons, U.S. Geological Survey, 345 Middlefield Road, MS 999, Menlo Park, CA 94025, USA. (tparson@usgs.gov)